Investigations for particulate processes relevant to pharmaceutical drug manufacturing

Anwesha Chaudhury *

External Supervisor: Prof. Johannes Khinast and Georg Scharrer

Research Center Pharmaceutical Center (RCPE)

Inffeldgasse 13, Graz, Austria 8010

Internal Supervisor: Prof. Rohit Ramachandran

Rutgers-The State University of New Jersey

98 Brett Road, Piscataway, NJ-08854

*Corresponding author: Anwesha Chaudhury, e-mail: *anwesha@eden.rutgers.edu*

Acknowledgement

First and foremost, I would like to thank the Marshall Plan foundation for giving me this opportunity to work in RCPE/ TUGraz, Austria. This exposure has led to a great enrichment in my research and my knowledge in the field. I have grown as a person as well as a researcher. I really appreciate this effort by the Marshall Plan foundation to encourage research exchange between the two countries-United States of America and Austria.

I would like to acknowledge Prof Johannes Khinast at RCPE (Research Center Pharmaceutical Engineering), Graz, for all of the invaluable assistance and guidance that he provided during my stay at Graz. Furthermore, I wish to thank Georg Scharrer for his unwavering support and assistance during this project, without which I would have been lost. I am indebted to Karin Leber, Kathrin Manninger and Margarete Hermann for their help in making sure that my time in Austria was as comfortable as possible, and for going out of their way in order to assist me with any issues I faced during my stay there. This work would not be possible without contributions from my colleagues in RCPE, whose support and friendship ensured that my time in Graz was filled with friendship and company, in addition to being academically fulfilling. I would like to especially thank my colleague Maximilian Besenhard, who has significantly contributed towards the parameter estimation study and this work would have been incomplete without his help and support. I would also like to express my gratitude towards Dr. Sharareh Salar Behzadi without whose support and guidance, the experimental work would have been impossible. My belief that collaborative work brings fruitful results has been reaffirmed after this experience.

I would also like to thank my friends and colleagues in Rutgers University who constantly supported me with my research and have been my pillar of hope through all ups and downs.

I would like to thank Dr. Yee Chiew at Rutgers University for helping and supporting me throughout the entire process of application for the Marshall plan scholarship. Finally, I would like to thank my advisor at Rutgers University, Dr Rohit Ramachandran, for his constant support of my research during my PhD, whose guidance has given me the tools and opportunity to travel to Graz and work with my peers there to research improved models for granulation, effective parameter estimation and have an experience to conduct experimental studies.

Contents

Abstract

This paper deals with the development of a new/novel, integrated model for a granulation process using population balance models (PBMs) and a detailed review on the effective parameter estimation for PBM based crystallization models. The model developed with regard to granulation process is an attempt on the author's part to connect the strong interactions between the various mechanisms involved in granulation that affects the final granule property. A novel aggregation kernel has been proposed which is semi-mechanistic in nature, yet computationally inexpensive. The PBMs for such particulate processes involve various empirical estimation which require effective estimation techniques. A detailed comparison has also been performed for the effective parameter estimation for improved predictability of the PBMs representing pharmaceutically relevant processes. Experimental studies have also been conducted for the fluid bed granulation process. This enhances the understanding of the effect of the various process parameters on the various mechanisms governing the pharmaceutical fluid bed granulation.

Keywords: Granulation, Crystallization, Multi-dimensional Population Balance Model, Aggregation, Breakage, Experimental studies, Parameter estimation

1 Introduction

Wet granulation is a crucial particle design process relevant to various particulate industries, which involves agglomeration of fine powder to form larger granules with the addition of external binder (Iveson et al., 2001). Granulated particles show improved flowability, reduction in the segregation of mixture, improved compressibility, controlled dissolution. Due to the lack of knowledge in processes involving solids, granulation is carried out in a very inefficient way in the industry with large recycle ratios (Salman et al., 2007). This necessitates the need to develop higher fidelity models in order to obtain better process knowledge, higher predictability and improved control and operation of the granulation process. From a similar perspective, development of sophisticated modeling techniques for the predictability of crystallization processes (crucial from a separation, size distribution and purification aspect) is yet another vital task to the pharmaceutical drug manufacturing. For instance, the proper regulation and control of such particulate processes in the pharmaceutical industry is of critical importance due to the imposition of a tight quality criteria by the regulating authorities (Reklaitis et al., 2010; Boukouvala et al., 2011a,b).

Using PBMs to model particulate processes such as granulation and crystallization is a well accepted practise prevalent in the scientific community (Litster, 2003; Iveson et al., 2001; Ramachandran et al., 2008a; Marchal et al., 1988; Gunawan et al., 2004; Oullion et al., 2007; Nagy, 2008). The biggest point that gives an edge to PBMs over other modeling approaches is the discrete nature of the PBEs which can very well capture the physics of the particulate processes and can reflect the finer underlying details. PBEs can be solved using various approaches such as finite element methods (Mantzaris et al., 2001), the method of

moments (Hulburt and Katz, 1964), the method of characteristics (Qamar and Warnecke, 2007; Mesbah et al., 2009), high resolution algorithms (LeVeque, 2002), hierarchical two tier technique (Immanuel and Doyle III, 2003; Pinto et al., 2007), Lattice Boltzmann approach (Majumder et al., 2012), Monte Carlo methods (Braumann et al., 2010; Marshall Jr et al., 2010; Marshall Jr. et al., 2011). Reduced order PBMs have also been studied by breaking the multidimensional PBM into multiple one-dimensional PBEs using the marginal distribution approach in order to obtain an equivalent system with less complicated numerical solution (Hounslow et al., 2001; Biggs et al., 2003). Many one dimensional PBMs have been reported in literature (Kapur and Fuerstenau, 1969; Sastry, 1975; Costa et al., 2007) which usually utilize granule size as the only independent property affecting the granule growth behavior. The inadequacy of considering one-dimensional models for granulation has been previously reported by Iveson (2002). He had suggested that for granulation, granule binder, porosity and in some cases, composition can vary between granules and thus needed to be addressed with the use of multidimensional PBEs alongwith the appropriate choice of internal coordinates and more accurate submodels.

The multidimensional PBM for granulation is formulated based on the individual solid, liquid and gas volumes as the internal coordinates in order to enable decoupling of the integrated process with respect to the individual meso-scopic subprocesses (Verkoeijen et al., 2002). The various underlying mechanisms (as shown in Figure 1) governing granulation, such as aggregation, breakage, drying/rewetting, consolidation, layering, have strong interactions with each other. Most models observed in literature have failed in tracking the induction behavior that exist in the granulation process. There is also a dearth of models

which can effectively address the interactions between the various subprocesses affecting the final outcome of granulation.

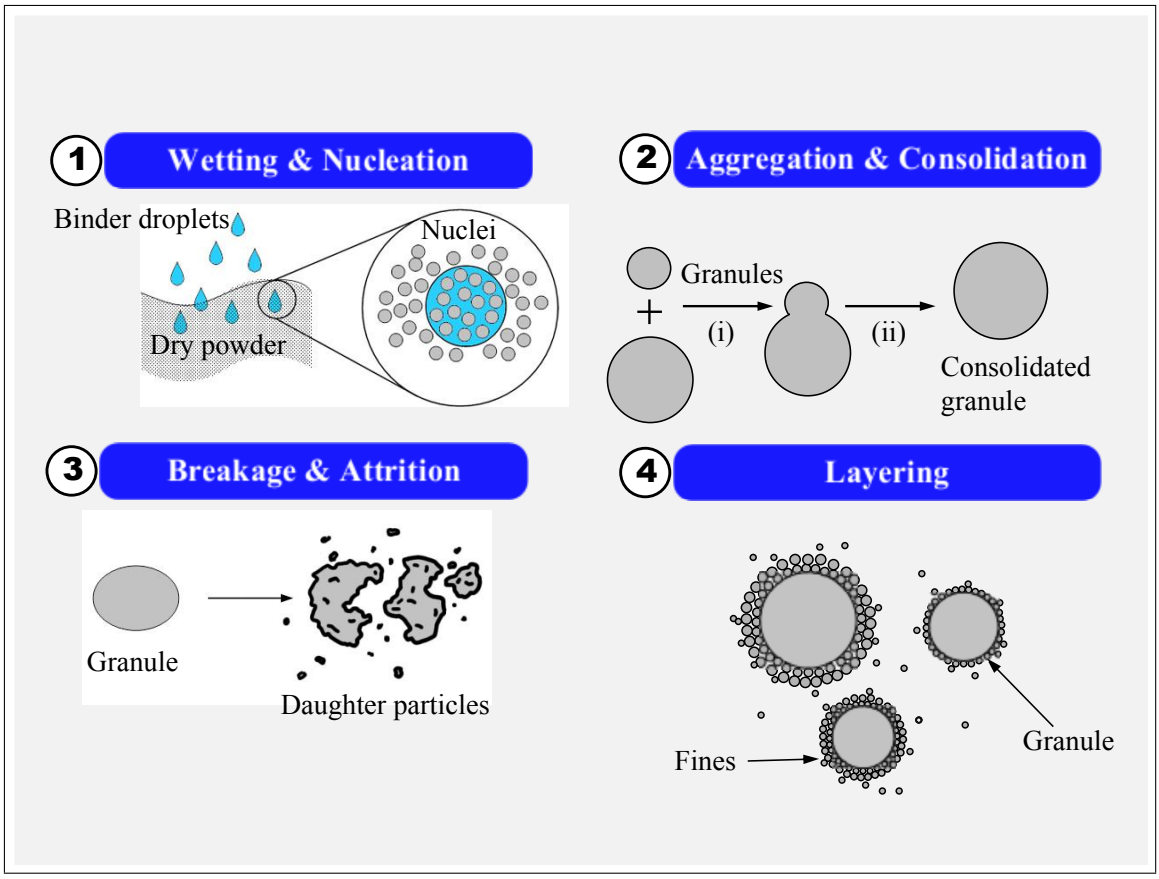

Figure 1: Various subprocesses affecting the final granulation outcome

The importance of multidimensional PBMs is already known to us (Iveson et al., 2001), but framing the model in a way, such that, the interactions can be tracked effectively, is a more challenging task. The significance of binder content in the growth of granules is associated with the fact that with higher amount of the binder, there is a larger availability of surface-wet granules (Knight et al., 1993) and that enhances the aggregation of finer particles (Link and Schlunder, 1997). As for the granule porosity is concerned, below a certain critical porosity, liquid is squeezed onto the surface, thus resulting in surface-wet granules which helps promote granule growth, hence porosity is an important particle trait that needs

to be characterized (Ramachandran et al., 2008b). With the progress of consolidation, more liquid is forced to squeeze out of the pores thus providing an increased surface liquid availability. So, as the impeller speed increases, the consolidation of particles increases and so does the aggregation and the breakage. The system is observed to exhibit steady growth when aggregation is more dominant. On the contrary, a less aggregation system is prone to exhibiting induction behavior (as aggregation is catalysed with the liquid being squeezed out of the pores as consolidation proceeds) under high consolidation (Walker, 2007). This work involves the identification of crucial operating parameters that critically affect the granulation process and expression of the mechanisms in terms of these measurable quantities. Therefore, these mechanisms can be said to be affected by the more fundamental operating properties such as rpm, granulator geometry and binder properties. Granulation can be carried out in a high shear, drum or fluid bed equipment in a batch mode.

One of the major drawbacks of using PBMs to quantify the behavior of the granulation process is the potential usage of empirical parameters. It is very important to use more mechanistic equations in order to have a more first principle based predictive model. Empirical aggregation (Adetayo and Ennis, 1997; Madec et al., 2003) and breakage kernels (Pandya and Spielman, 1983) have been more commonly observed in literature, but these kernels cannot be used for extrapolating the system behavior under different operating conditions and neither be utilized for predictive understanding of the process. Immanuel and Doyle III (2005) had proposed a mechanistic kernel, based on the coalescence mechanisms identified by Liu et al. (2000) and Ennis et al. (1991), which can be considered to be a more fundamental representation of the granulation process as it takes into account the effect of key material

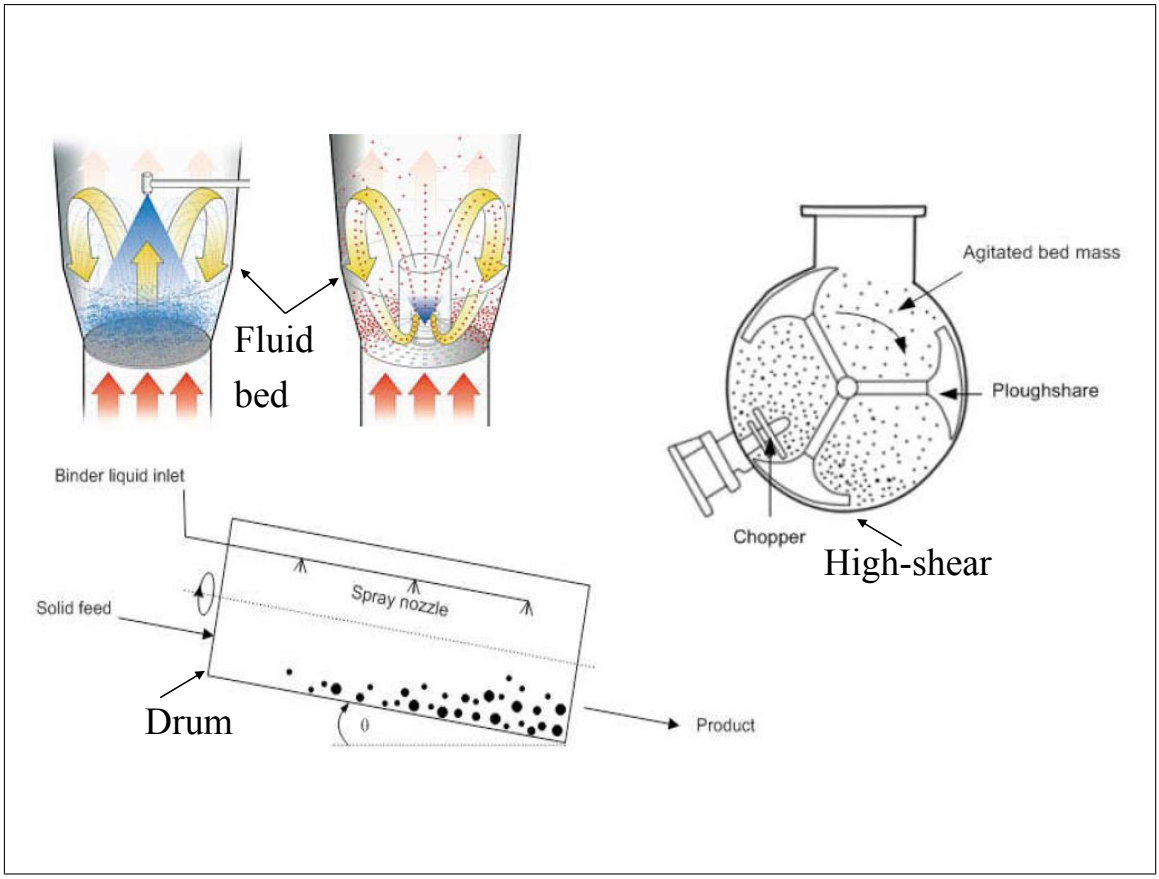

Figure 2: Various granulation equipments in batch mode

properties and process parameters. Various other experimental studies have been carried out in order to link the process variables and various microscopic properties of the particles with the granulation process (Liu et al., 2000; Stepanek and Rajniak, 2006). Similarly, a more fundamental breakage kernel was proposed by Ramachandran et al. (2009) which gives a better insight into the breakage mechanism. In this work we have proposed a semi empirical aggregation kernel which takes into account the effects of critical parameters such as contact angle, binder properties and the rpm of the granulator. Other considerations taken into account are the inhomogenities related to binder distribution, which has been addressed using a compartmental based model. An attempt has also been made to express the various mechanisms as a function of the operating parameters which can be manipulated

for controlling the process outcome.

In spite of using mechanistic equations for describing the various mechanisms governing the granulation process, usage of empirical parameters can be reduced but not totally abolished. For this purpose, a 1-D PBM describing crystallization has been utilized for a detailed review on the popular parameter estimation techniques considering an inverse problem. This study is aimed at providing a better insight on the parameter estimation techniques which can be later extended for the multidimensional PBM representing the granulation process. The main impetus behind this work is to connect the interactions between the mechanisms influencing granulation so that a better physical representation can be derived which can also enable improved control studies. Effective parameter estimation techniques also enhance the ability of the developed model to predict the real outcome of the process. Several techniques have surfaced in the past years which propose an efficient optimization algorithm for the accurate estimation of empirical parameters. The implementation of a weighted least square objective function comprising of the estimated and the experimental data was considered in the works of (S. and Ken, 1990; Tadayon et al., 2002). Some work has been observed with the implementation of SQP (sequential quadratic programming) for the parameter estimation of crystallization processes (Kalbasenka et al., 2011). Gradient based methods were employed with the help of NAG libraries in FORTRAN for fitting the experimental concentration and CSD data using splines by (Qiu and Rasmuson, 1991). Hu et al. (2004) had considered a maximum likelihood function for the estimation of parameters using the concentration and CSD, and the covariance matrix for testing the robustness of their approach. A similar objective function was considered by Matthews and Rawlings

(1998) for the parameter estimation procedure followed by incorporating the SQP algorithm for the optimization. Optimal control problems in crystallization were previously studied by Seki et al. (2012); Modares and Sistani (2011) using the particle swarm algorithm with slight improvements. Reche-Lopez et al. (2009) had published an informative paper with the comparison of the various meta-heuristic methods for the optimization of the biomass power plants. In the past decade, using the dynamic optimization algorithm of gPROMS for parameter estimation of PBEs for crystallization processes has been observed to be quite popular (Nowee et al., 2007; Widenski et al., 2011). We have performed a comparative study with the metaheuristic optimization techniques-Simulated Annealing (SA), Particle Swarm algorithm (PSO) and the dynamic optimization algorithm implemented by PSE (Process Systems Enterprise) in gPROMS.

The proposition of this work can be foreseen as a very good platform for improved control and optimization studies. The model enables the quantification of the various mechanisms individually, but as a function of the presence of other mechanisms acting simultaneously. Some experimental investigations have also been performed using a fluidized bed equipment for granulation in order to get a better insight on the effect of the various operating parameters. Advantages of fluid bed granulation over other granulation methods are usually indicated to be higher product density, and lower solvent and energy consumption (Boerefijn and Hounslow, 2005). Fluid bed granulation is an inherently complex process consisting of many interconnected process variables that are available at the operator's disposal in obtaining a suitable recipe for achieving good granulation. The granulation process in a fluid bed requires a binary nozzle, a solution delivery system and compressed air to atomize the liquid

binder. When the binder liquid is sprayed on to a fluid bed, relatively loose and porous granules are formed.

For a fluid bed process, binder content and the particle/excipient solubility have an important role to play in the granulation process (Rajniak et al., 2007). The mode of binder addition also has a major role to play in the formation of granules in wet granulation (Reynolds et al., 2004).Non-uniformity of binder distribution is common in granulation and studies have been conducted to address this heterogeneity in case of a fluid bed process (Osborne et al., 2011). Various other exper- imental studies have been carried out in order to link the process variables and various microscopic properties of the particles with the granulation process (Liu et al., 2000; Stepanek and Rajniak, 2006). Aside from porosity and bed humidity, other granule properties such as the Hausner index and the angle of repose were also evaluated with the help of optimal experimental design (Rambali et al., 2003). Information on the pneumatic behavior of the system undergoing fluid bed spray granulation has also been obtained from Morl et al. (2007). The granule size distribution is also dependant on the surface characteristics of the particle. Studies have shown that hydrophilic particles show a more narrow particle size distribution as compared to hydrophobic particles (Thielmann et al., 2008). Other simpler heat and mass balance based models have also been developed in order to obtain the wettability, temperature and concentration distribution of the particles (Heinrich and Morl, 1999). The biggest challenge with conducting granulation in a fluid bed equipment is the complex intertwined effect of the multiple operating parameters (such as product temperature, air flowrate, liquid spray rate and so on) that affect the process.

2 Mathematical modeling for granulation

2.1 Model Formulation

The 3-D PBE, based upon our previous works (Poon et al., 2009; Ramachandran and Barton, 2010; Ramachandran et al., 2012; Chaudhury et al., 2012), describing granulation process can be written as

$$\frac{\partial}{\partial t}F(s,l,g,t) + \frac{\partial}{\partial g}\left[F(s,l,g,t)\frac{dg}{dt}\right] + \frac{\partial}{\partial s}\left[F(s,l,g,t)\frac{ds}{dt}\right] + \frac{\partial}{\partial l}\left[F(s,l,g,t)\frac{dl}{dt}\right] = \Re_{aggregation} + \Re_{breakage} + \Re_{nucleation} \quad (1)$$

where $F(s,l,g,t)$ represents the population density function. The solid, liquid and gas volumes have been represented with the variables s, l and g. The respective partial derivative terms represent the various growth mechanisms-layering,rewetting/drying and consolidation, associated with the granulation process. An integrated model containing the various mechanisms significant in a fluid bed granulation process, such as aggregation, breakage, liquid distribution and consolidation has been considered for the purpose of a detailed analysis. Nucleation and layering has been ignored in this work but can be easily incorporated.

Aggregation is the phenomenon in which smaller particles collide to form a larger particle in the presence of surface binder that acts like a liquid bridge between the two smaller mother particles. This involves the loss of two or more particles in the smaller bin to give birth to one large aggregate in a larger bin. The overall aggregation can thus be broken into the

corresponding birth and death terms as

$$\Re_{agg}(s,l,g) = \Re_{agg}^{form} - \Re_{agg}^{dep}, \tag{2}$$

such that,

$$\begin{aligned}\Re_{agg}^{form} = \frac{1}{2}\int_0^{s_{max}} \int_0^{l_{max}} \int_0^{g_{max}} \beta(s', s-s', l', l-l', g', g-g') \\ \times F(s', l', g', t) F(s', s-s', l', l-l', g', g-g', t) ds' dl' dg'\end{aligned} \tag{3}$$

$$\begin{aligned}\Re_{agg}^{dep} = F(s,l,g,t)\int_0^{s_{max}} \int_0^{l_{max}} \int_0^{g_{max}} \beta(s', s-s', l', l-l', g', g-g') \\ \times F(s', l', g', t) ds' dl' dg'\end{aligned} \tag{4}$$

where, $\beta(s', s-s', l', l-l', g', g-g')$ is the aggregation kernel that governs the rate at which two granules of internal coordinates (s', l', g') and $(s-s', l-l', g-g')$ agglomerate.

Breakage is the process of disintegration of larger particles into smaller fragments due to various external forces from the particles hitting the walls, another particle or the impeller. When these forces exceed the intrinsic strength of particles, breakage of particles result. Thus breakage involves the loss of one particle in the larger bin and the emergence of two or more smaller particles in the smaller bins. Using this information, the breakage term can be broken into its corresponding birth and death terms as

$$\Re_{break}(s,l,g) = \Re_{break}^{form} - \Re_{break}^{dep}, \tag{5}$$

such that the birth and death terms can be explained using Equations (6) and (7)

$$\Re_{break}^{form} = \int_0^{s_{max}} \int_0^{l_{max}} \int_0^{g_{max}} K_{break}(s,l,g) b(s', s-s', l', l-l', g', g-g') \times F(s', l', g', t) ds' dl' dg' \tag{6}$$

$$\Re_{break}^{dep} = K_{break}(s,l,g) F(s,l,g,t). \tag{7}$$

Consolidation is a negative growth process which represents the compaction of granules as air escapes out of the pores. It can modeled as an empirical exponential decay relation (Verkoeijen et al., 2002) given by

$$\frac{d\epsilon}{dt} = -c(\epsilon - \epsilon_{min}), \tag{8}$$

$$\frac{dg}{dt} = \frac{C_{con}(s+l+g)(1-\epsilon_{min})}{s} \times [l - \frac{\epsilon_{min} s}{1-\epsilon_{min}} + g] \tag{9}$$

where, the porosity ϵ is

$$\epsilon = \frac{l+g}{s+l+g} \tag{10}$$

Here ϵ_{min} is the minimum porosity of the granules and c is the compaction rate constant. From literature, it has been observed that the consolidation of particles increases with increasing rpm of the impeller (Rahmanian et al., 2011). The effect of consolidation saturates beyond a certain impeller speed. Therefore, in this work it has been approximated as a weak exponential function of the impeller rpm as

$$C_{con} = k_{con} \times e^{\left(\frac{rpm}{1000}\right)} \tag{11}$$

Drying/rewetting denotes the increase or decrease of liquid content into or from the granulation system due to addition of binder or removal due to evaporation. For the sake of simplicity, we have neglected the evaporation term ($\dot{m}_{evap} = 0$) in this work. The liquid water balance (Chaudhury et al., 2012) can be written in (12) as

$$\frac{dl}{dt} = \frac{\dot{m}_{spray}(1 - c_{binder}) - \dot{m}_{evap}}{M_{solid}}, \tag{12}$$

where,

$$M_{solid} = M_{solid\ fraction} + \dot{m}_{spray} c_{binder} \Delta t, \tag{13}$$

Non-uniformity of binder distribution is common in granulation and studies have been conducted to address this heterogeneity in case of a fluid bed process (Osborne et al., 2011). Models have been developed to obtain the surface availability of moisture of granulation purposes (Ronsse et al., 2012), which can be incorporated in the mechanistic kernel in order to obtain and aggregation kernel with more system information embedded in it. The inhomogeniety associated with binder addition has been tackled using a compartmental based model. In this work, we have subdivided the granulator into two compartments, however using more compartments would enable us to track the inhomogeniety better and will give a better representation of the real scenario. A compartment based model similar to the works of Li et al. (2012) and Wnukowski and Setterwall (1989) was adopted in order to represent the inhomogeniety associated with the binder distribution. Two compartments have been

considered with the corresponding number distribution of particles as F_1 and F_2. Compartment 1 is considered the spray zone which recieves 70 percent of the total liquid added and compartment 2 is the bulk zone that is assumed to receive the remaining 30 percent of the total liquid. The particles spend less time in the spray zone and the portion of the entire population enclosed in the compartment depicting the spray zone is α_1 and that for the bulk zone is α_2. There is also believed to be be a circulation between the two compartments thus leading to an open system with exchange of powder and this rate is depicted as a.

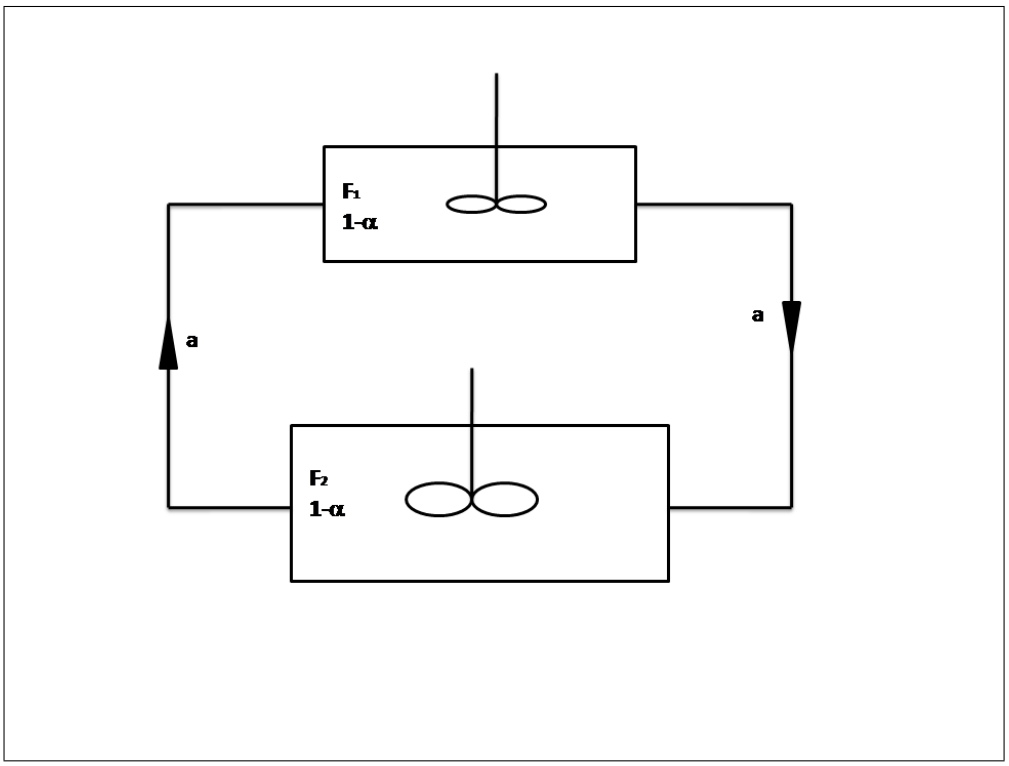

Figure 3: Schematic of the compartmental model for binder distribution (Li et al., 2012)

Including the compartment based model, our PBM can be written in the form as shown in Equations 14

$$\frac{\partial F_1}{\partial t} + \frac{\partial}{\partial g}\left[F_1 \frac{dg}{dt}\right] + \frac{\partial}{\partial s}\left[F_1 \frac{ds}{dt}\right] + \frac{\partial}{\partial l}\left[F_1 \frac{dl}{dt}\right] = \Re_{1,aggregation} + \Re_{1,breakage} + \Re_{1,nucleation} - a\left(\frac{F_1}{1-\alpha} - \frac{F_2}{\alpha}\right)$$

$$\frac{\partial F_2}{\partial t} + \frac{\partial}{\partial g}\left[F_2 \frac{dg}{dt}\right] + \frac{\partial}{\partial s}\left[F_2 \frac{ds}{dt}\right] + \frac{\partial}{\partial l}\left[F_2 \frac{dl}{dt}\right] = \Re_{2,aggregation} + \Re_{2,breakage} + \Re_{2,nucleation} + a\left(\frac{F_1}{1-\alpha} - \frac{F_2}{\alpha}\right) \quad (14)$$

In this work, we have also made an attempt to derive a simplistic yet mechanistic aggregation kernel which could be expressed as a function of the more crucial operating parameters such as the rpm of the impeller, the binder properties (viscosity, surface tension) and the contact angle. The details about the aggregation kernel will be proposed in the subsection 2.2

2.2 Aggregation kernel

From literature, it has been observed that some of the crucial parameters affecting aggregation are the impeller speed (Nursin, 2010), binder viscosity (Iveson et al., 2001), contact angle and the amount of surface liquid (Immanuel and Doyle III, 2005). The binder viscosity influences the Stoke's criterion that has been previously used for various works that has studied the aggregation of powder (Stepanek et al., 2009). The contact angle of the binder liquid influences the wetting of the particle surface by the liquid and hence gives an idea about the amount of wetted area and liquid depth available on the particle surface. The wetted area and the liquid depth are crucial parameters that affect the aggregation of particles.

For this study, we have considered the system to operate under the drop controlled regime where a single droplet hits one particle. Also, from the works of Hapgood et al. (2002, 2009), we can obtain the volume of liquid on the surface of a porous particle at various time instants as

$$V(t) = V_0 - \pi R_d \epsilon \sqrt{\frac{\gamma_{LV} R_{pore} cos\theta}{2\mu} t} \tag{15}$$

Where, V(t) is the volume of liquid on the surface at time, t, R_d is the radius of the droplet, ϵ is the porosity, γ_{LV} is the surface tension of the liquid, μ is the viscosity of the liquid, θ is the contact angle and R_{pore} is the radius of the pore that can be written as $R_{pore} = \frac{d_{32}}{3}\frac{\epsilon}{1-\epsilon}$. Due to addition of liquid during the wet massing period, the volume does not remain constant, so we quantify the surface liquid as

$$V(t) = max\left(V(t-1) - \pi R_d \epsilon \sqrt{\frac{\gamma_{LV} R_{pore} cos\theta}{2\mu} \delta t}, 0\right) + V_{drop} \tag{16}$$

In our study, we have used a constant contact angle, although in real scenario, the contact angle varies over time and is dynamic in nature following the Young-Dupre's equation. The dynamic contact angle could be expressed as a function of the surface tension and the friction coefficient (Seveno et al., 2002). The drop penetration time described in previous works by Hapgood et al. (2003) also gives an idea on the amount of time required by a droplet to completely sink into a particle pore. The radius of the area wetted as a single droplet hits the surface can be given as,

$$R_{wet} = \frac{3V}{\pi}\Phi(\theta) \tag{17}$$

where,

$$\Phi(\theta) = \frac{sin^3(\theta)}{2 - 3cos(\theta) + cos^3(\theta)} \tag{18}$$

The area of the particle surface wetted by a droplet can be calculated by evaluating the area of a circle having a radius of R_{wet} (assuming the surface to be flat and ignoring the curvature). As time proceeds, more and more droplets hit the particles. So at time, t, the area wetted by the droplets can be considered as $N \times A_{wet}$, where N is the number of droplets that have hit the particle and to take some overlap of droplets into consideration, an overlap factor, k is also multiplied. This also translates to the sigmoidal function that was approximated by Stepanek et al. (2009) in his previous works. The final equation can be written as shown in Equation (19).

$$A_{wet}(t, s, l, g) = \pi \times R_{wet}^2 \times N \times k \tag{19}$$

The liquid sinks into the particles as long as the pores are not filled. Once the pores get filled to its saturation point, the excess liquid remains on the surface and contribute to higher aggregation of particles. The depth of the surface liquid, h_0 present can be expressed as a function of the volume and the wetted area as

$$h_0(s, l, g) = 1.5 \times \frac{V(t, s, l, g)}{A_{wet}(s, l, g)} \tag{20}$$

The surface asperity, h_a is considered to be 0.2 times the particle diameter. Using these information, the aggregation kernel is considered to be a product of a size dependant part and a size independent part. The aggregation kernel can be represented as

$$K_{agg}(s,l,g,s-s',l-l',g-g') = B_0\Psi(s,l,g,s-s',l-l',g-g') \times \tag{21}$$

$$A(s,l,g,s-s',l-l',g-g') \times \beta_0(s,l,g,s-s',l-l',g-g')$$

Where, $\Psi(s,l,g,s-s',l-l',g-g')$ is a binary variable representing the Stoke's criterion and can be written as expressed in Equation (22), $A(s,l,g,s-s',l-l',g-g')$ is obtained from the fractional wetted area of the two aggregating particles and β_0 represents the size dependant part of the kernel. $\Psi(s,l,g,s-s',l-l',g-g')$ can be calculated from the Stoke's criterion as

$$\Psi(s,l,g,s-s',l-l',g-g') = \begin{cases} 1, & \text{if } St \leq St^* \\ 0, & \text{if } St \geq St^* \end{cases} \tag{22}$$

where, the Stokes number and the critical Stokes number can be written as a function of the particle velocity u_0, viscosity μ, average mass $\bar{m}$, average diameter $\bar{d}$, surface liquid depth λ_{12} and surface asperities h_a as

$$St = \frac{8\tilde{m}u_0}{3\pi\mu\tilde{d^2}}$$
$$St^* = 2ln\frac{\lambda_{12}}{h_a} \tag{23}$$

The factor $A(s,l,g,s-s',l-l',g-g')$ represents the product of the fractional wetted

area of the two aggregating particles and can be written as

$$A(s,l,g,s-s',l-l',g-g') = \frac{A_{wet}(s,l,g)}{A_{total}(s,l,g)} \times \frac{A_{wet}(s-s',l-l',g-g')}{A_{total}(s-s',l-l',g-g')} \tag{24}$$

The size dependant part of the kernal can be expressed using the kernel proposed by Madec et al. (2003).

$$\beta_0 = (L_1^3 - L_2^3)\left((c_1+c_2)^\alpha \left(100 - \frac{c_1+c_2}{2}\right)^\delta\right)^\alpha, \tag{25}$$

where,

$$c = \frac{volume\ of\ surface\ liquid}{volume\ of\ agglomerate}100. \tag{26}$$

The final aggregation kernel is taken to be a product of all these variables which focus on the various aspects that influence the existance of a successful collision.

2.3 Breakage kernel

This work also takes into account the mechanistic breakage kernel proposed by Ramachandran et al. (2009) which relates the kernel to fundamental properties such as viscosity, surface tension, contact angle and volume fraction of the daughter particles formed. Sensitivity analysis showed that these quantities significantly influence the output of the process. The breakage kernel is said to be proportional to the ratio of the external stress, σ_{ext} to the intrinsic strength. The external stress is represented as

$$\sigma_{ext}(s,l,g) = \frac{F_{ext}(s,l,g)}{A_c(s,l,g)} \tag{27}$$

where F_{ext} is the external forces acting on the particle and A_c is the contact area. In order to evaluate the external forces and the contact area, various cases that influence the total force/contact area have been considered. This includes the forces due to fluid flow, particle-particle collisions,particle-wall collisions and particle-impeller collisions. For further details, the authors would like direct the readers to the works of Ramachandran et al. (2009). The intrinsic strength of the particle was found to be primarily influenced by the forces due to mobile liquid bridges. Using these information, the breakage kernel, K_{break} was finally expressed as

$$K_{break}(s,l,g) = f(\theta, \mu, \gamma, Young's\ modulus, fraction\ of\ volume\ of\ daughter\ particles) \tag{28}$$

Figures 4, 5, 6 reveals a comparative study of the semi-mechanistic kernel proposed by Soos et al. (2006), the empirical kernel proposed by Pandya and Spielman (1983) and the mechanistic kernel developed by Ramachandran et al. (2009). This study was shown in Ramachandran et al. (2009) and has been published thus justifying the use of a mechanistic kernel in place of including empiricity. The semi-empirical kernel proposed by Soos et al. (2006) can be expressed as

$$K_{break}(s,l,g) = \left(\frac{4}{15\pi}\right)^{\frac{1}{2}} \times G \times \left(-\frac{B}{G^2 R(s,l,g)}\right) \tag{29}$$

where, G is the shear rate, $R(s,l,g)$ is the radius of the particle and B is an empirical

constant. The empirical proposed by Pandya and Spielman (1983) can be written as

$$K_{break}(s,l,g) = P_1 G(R(s,l,g))^{P_2} \tag{30}$$

where P_1 and P_2 are empirical constants, G is the shear rate and $R(s,l,g)$ is the radius of the particle.

This way the granulation PBM was framed which took into account the inter-relationship between the various mechanisms that act as granulation proceeds.

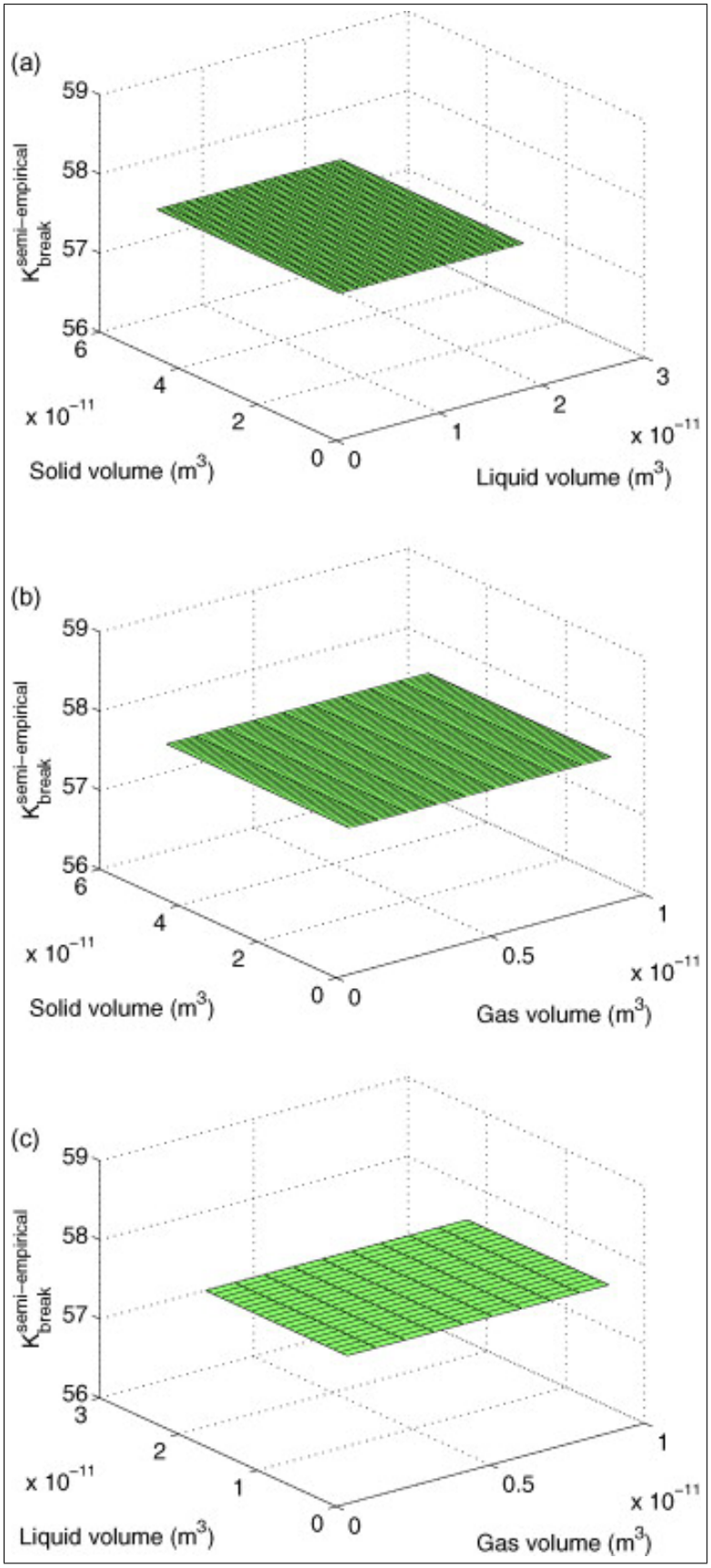

Figure 4: Shape of the semi-empirical kernel with respect to two dimensions keeping the third constant: (a) volume of gas constant, (b) volume of liquid constant and (c) volume of solid constant

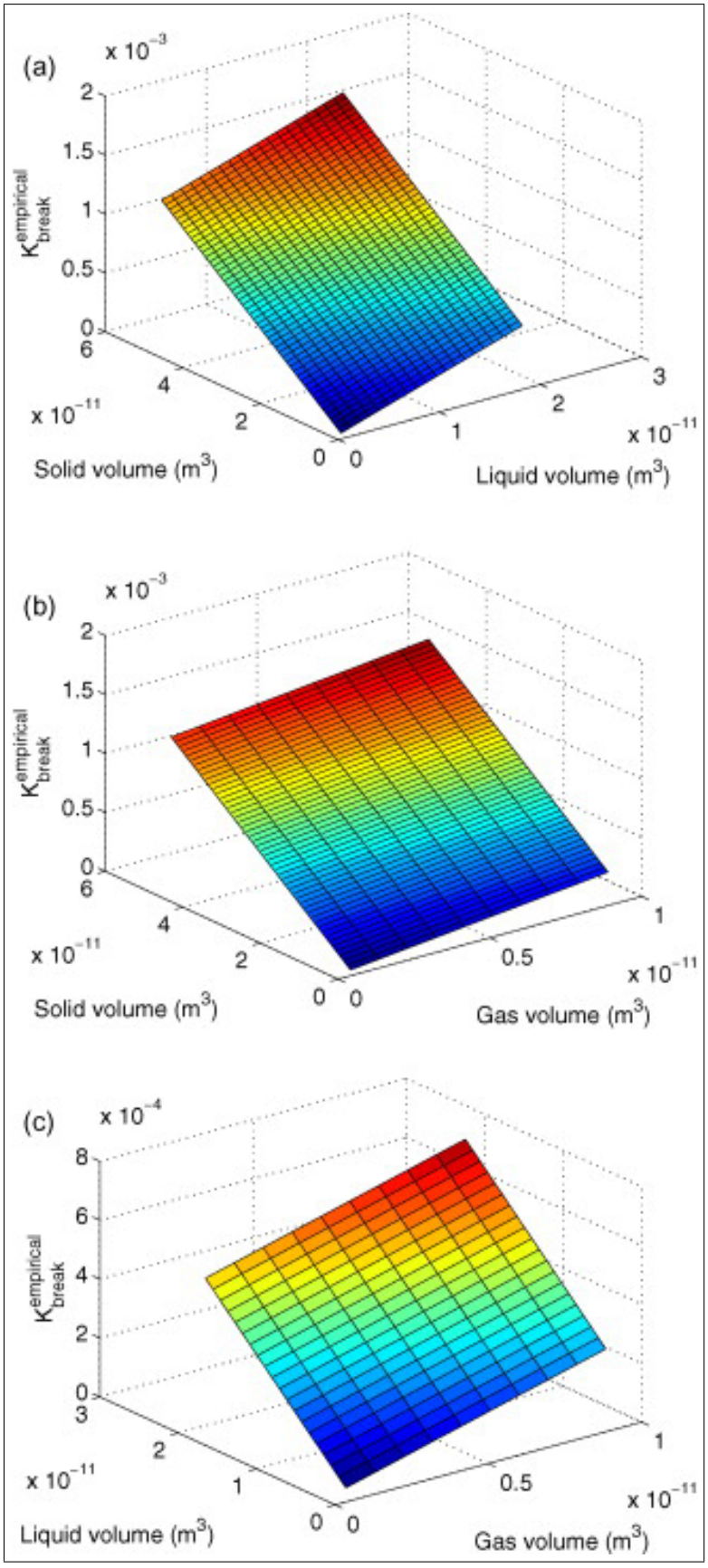

Figure 5: Shape of the empirical kernel with respect to two dimensions keeping the third constant: (a) volume of gas constant, (b) volume of liquid constant and (c) volume of solid constant

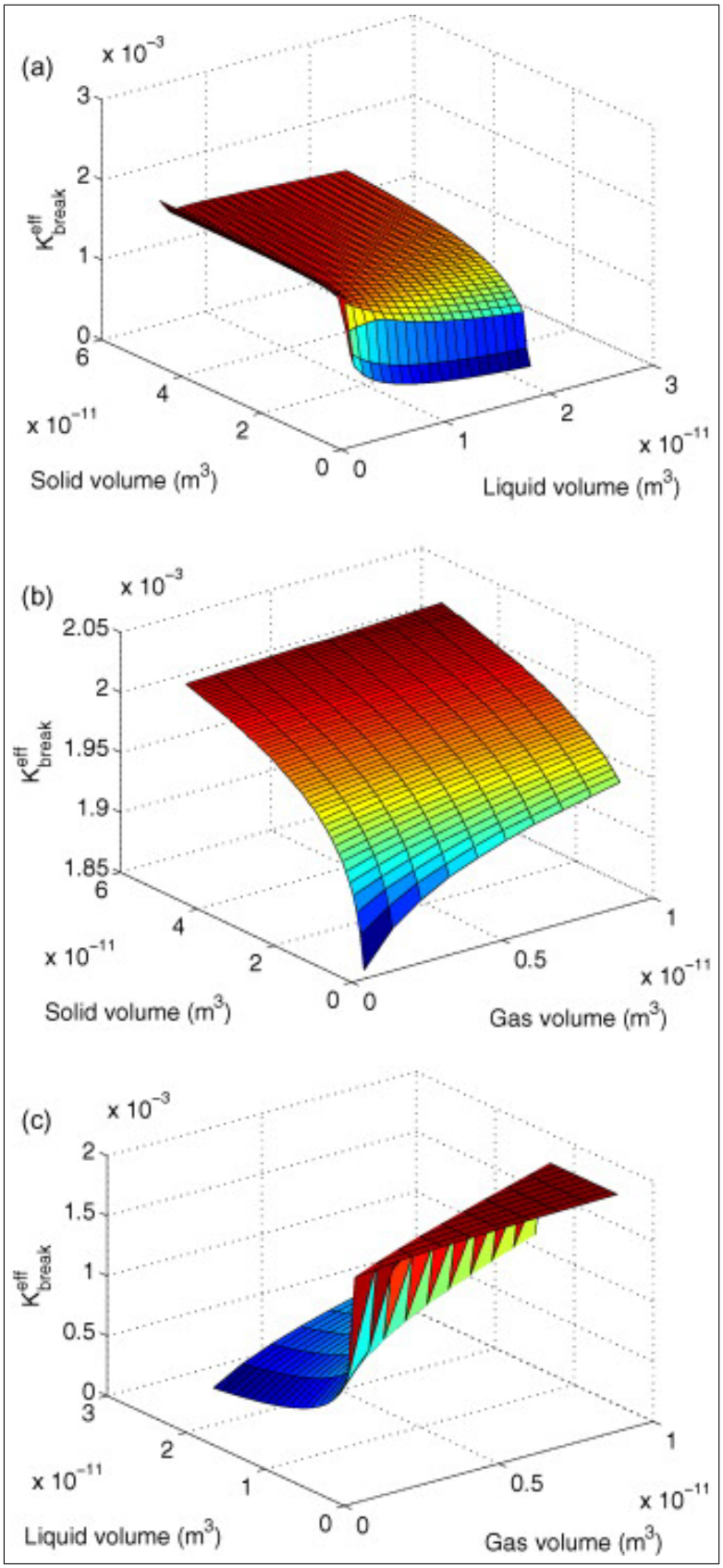

Figure 6: Shape of the mechanistic kernel with respect to two dimensions keeping the third constant: (a) volume of gas constant, (b) volume of liquid constant and (c) volume of solid constant.

3 1-D PBM for crystallization

3.1 Model development

The current work does not pertain to the crystallization of a specific substance. Nevertheless we would like to implement material attributes of well known substances to simulate a realistic process. The process model describes a (well mixed) seeded batch cooling crystallization process of a model API (API) in a model solvent (Sol). The model relevant material material constants and process setting are listed and described in Table 1

Table 1: Material constants and process settings

Material constants	**Value**	**Description**
Molecular weight of API	$MW_{API} = 180.16 g/mol$	Molecular weight of Acetylsalicylic acid (Aspirin)
Molecular weight of Solvent	$MW_{Sol} = 46.07 g/mol$	Molecular weight of Ethanol
Density crystalline phase Density pure solvent Density solvent with dissolved species	$\rho_{cp} = 1(kg/l)$ $\rho_{sol} = 1(kg/l)$ $\rho_{sol+ds} = 1(kg/l)$	We assume an equal density for the crystalline, pure solvent and the solvent containing dissolved species of the crystalline phase

To establish the solubility of our model API in our model solvent we used the solubility of acetylsalicylic acid dissolved in pure ethanol. The latter can be described by a Nyvlt model for the Temperature measured in Kelvin

$$log(X_{cp}) = N_1 + \frac{N_2}{T} + N_3 log(T) \tag{31}$$

with $N_1 = 27.769,\ N_2 = -2500.906$ and $N_3 = -8.323$ (Maia and Giulietti, 2008). In the

present work we use the supersaturation, S defined as

$$S = \frac{c\ [mol/l]}{c*\ [mol/l]} \tag{32}$$

where c^* is solubility of the API in the Solvent and c its current concentration. The conversion of the molecular fraction to the amount of moles per liter was performed according to Equation 33 which describes the latter for the initial process conditions

$$G(S,T) = k_1.exp\left(\frac{-k_2}{RT}\right).(S-1)^{k_3} \tag{33}$$

With the inverse problem consideration, the target values for the parameter estimation have been generated from simulations with known empirical parameters. The values for the various empirical parameters in Equation (33) are $k_1 = 10\ [m/s]$, $k_2 = 10^4\ [J/mol]$ and $k_3 = 1$.

In the present work we only consider experiments starting with the same mass ratio of API and Sol. Therefore the initial seed mass (non dissolved amount of the API being already in the crystalline phase) of the model API $m_{cpinitial}$ as well as the initial concentration of the dissolved species $c_{APIinitial}$ depends only on the solubility at the initial temperature $T_{initial}$.

$$C_{APIinitial}[mol/l] = \left(\frac{\rho_{sol+ds} X_{cp} T_{initial}}{MW_{cp}(X_{cp}T_{initial}) + (1 - X_{cp}T_{initial})MW_{sol}}\right).10^3 \tag{34}$$

$$m_{cp\ initial}[kg] = m_{cp} - c_{cp0}.MW_{cp}10^{-3} \tag{35}$$

The PBM for crystallization considering the growth only mechanism can be written as

$$\frac{\delta F(L,t)}{\delta t} + \frac{\delta G(L,t) f(L,t)}{\delta L} = 0 \tag{36}$$

The initial CSD is expressed as a logarithmic distribution written as

$$f(L) = \frac{1}{L\sigma_{ln}\sqrt{2\pi}} exp\left(-\frac{1}{2}\left(\frac{ln(L/L_{50})}{\sigma_{ln}}\right)^2\right) \tag{37}$$

with $\sigma_{ln} = 0.4$ and $L_{50} = 100\mu m$ to defining the seed crystal's CSD. Furthermore we assumed cubic crystals (for the entire process) and defined the length as the characteristic length for a particle defined by L. Therefore the total amount of particles of a specific size L could be computed from $m_{cpinitial}$ if we assume cubic particles by using the constraint

$$\int_0^{L_{max}} f(L) L^3 \rho_{cp} =^{def} m_{cp\ 0} \tag{38}$$

Five different experiments with different initial concentrations $c_{API}[mol/L]$ and cooling rates col.rate are simulated to produce data necessary for estimation of kinetic parameters. The process time was set to end the cooling crystallization process at $T_{end} = 25^0 C$. If surface integration or diffusion to the surface is the limiting factor in crystal growth depends on material itself, its solubility in the used solvent and the supersaturating level. Growth mechanisms and therefore the adequate mathematical representation of the growth rate changes from surface integration limited to diffusion limited if the super saturation increases. Therefore, we designed experiments in which the supersaturation does not exceed a level of $S = 1.5$. We assume that our growth rate mechanism is surface integration limited for which

the Equation (33) is valid. The process setting of the simulated experiments are listed in Table 2

Table 2: Process settings for the simulated experiments

Experiment	$T^0_{initial}C$	$m_{cp\ initial}[kg]$	$coolingrate[^0C/s]$	$t_{process}[s]$
1	45	0.348	0.005	4000
2	45	0.348	0.025	800
3	55	0.428	0.025	1200
4	55	0.428	0.005	6000
5	50	0.388	0.015	1666

3.2 Optimization algorithms

In this section, a brief overview is provided on the theory and implementation of the various algorithms for the purpose parameter estimation. The value for the empirical parameters are bounded using an upper and a lower bound. The range for the parameters is $0 < k_1 < 500,\ 0 < k_2 < 100000$ and $0 < k_3 < 10$.

To avoid redundant computational effort, unrealistic combinations for $k_1,\ k_2,\ k_3$ have not been tested (not accepted in the case of SA, see section Simulated Annealing Algorithm, or not made g_{best} or b_{best} in the case of PSA, see section Particle Swarm algorithm). To test if a combination of k_1, k_2, k_3 could be assumed to be unrealistic, the growth rate G (equation 2) for a level of supersaturation of $S = 1.1$ and a temperature of $T = 30^0C$ was calculated first and compared to a rough estimation of the growth rate for these parameters $G_{estimation}$. $G_{estimation}$ was roughly estimated from the average crystal size $\bar{L}$ of the seeds CSD and those of the product crystals at the end and the process time $t_{process}$

$$G_{estimation} = \frac{\bar{L}_{seed} - \bar{L}_{product}}{t_{process}} \tag{39}$$

An estimation of the growth rate from data of simulated experiments as described above yields a value of $G_{estimation} = 4 \times 10^(-4)[(\mu m)/s]$. Before the model was executed in the presented optimization algorithms, the new parameters k_n were tested on reasonability according to the following constraints:

$$G(S = 1.1, T = 30|k_n) < 1000 G_{estimation}$$

$$G(S = 1.1, T = 30|k_n) 1000 > G_{estimation} \tag{40}$$

$$\tag{41}$$

The parameters were not tested if these constraints had been violated. Although the estimation of the growth rate at fixed values of supersaturation and temperature from experiments in which the temperature and the supersaturation are alternated is not feasible, the constraints we made should be valid as we set the scope to three orders of magnitude.

Objective function

In the case of the stochastic algorithms (Simulated Annealing Algorithm and Particle Swarm Algorithm) the estimation problem was minimized according to the objective function

$$\phi(\theta) = \sum_{i=1}^{a} \sum_{j=1}^{b} \omega_{ij} (\hat{Y_{ij}} - Y_{ij})^2 \tag{42}$$

where $\hat{Y_{ij}}$ and Y_{ij} are the measurement and model prediction of the of the j^{th} measured

variable at the i^{th} experiment, ω_{ij} is a weighting factor, b the number of measured variables and a the number of experiments.

In the case of the growth only assumption we used the concentration values to $\hat{Y_{ij}} = c_{ij}[mol/L]$ and weighted all concentration experiments for the considered experiments equally $omega_{ij} = 1$

3.2.1 Simulated Annealing Algorithm (SAA)

Simulated annealing is an algorithm that originates in material science engineering, originally introduced to find the equilibrium configuration of a collection of atoms at a given temperature when a liquid is freezing and crystallize during an annealing process (Metropolis et al., 1953). The algorithm was first used for solving optimization problems by Kirkpatrick et al. (1983) The concept of SA is to find the global minimum by simulating a slow cooling process on the computer. To this end we introduce an artificial temperature T_{SA} and a probability distribution $p_E(x|T_{SA})$, the so called acceptance distribution for a given configuration x at a given artificial temperature T_{SA}. The objective function to be minimized is denoted by $\Phi(x)$. According to classical SA we choose

$$p_E(x|T_{SA}) = \frac{1}{Z} e^{\frac{-\Phi(x)}{T_{SA}}} \tag{43}$$

which corresponds to a Boltzmann distribution with a normalization factor Z. The purpose of p_E is to assign a high probability to states with the objective function is small, i.e. states x close to the global minimum. A random walker will spend more time near the optimum states. The possibility for the walker also to go uphill and leave a local minimum,

which makes SA a global optimization technique, is therefore depending on T_{SA}.

Classical simulated annealing (CSA) involves three steps

1) **Generation of states**

Here the new states x_n in the parameter space were generated from the current x_c according to a Gaussian.

$$p(\Delta x_i = x_{i\ c} - x_{i\ n}) = \frac{1}{\sigma_i \sqrt{2\pi}} e^{-\frac{1}{2}\frac{\Delta x_i}{\sigma_i}^2} \tag{44}$$

2) **Acceptance of states**

We chose the Metropolis probability to accept or deny the generated new states. We define an acceptance probability of

$$p_{accept} = min\left[1, \frac{p_E(x_n|T_{SA})}{p_E(x_c|T_{SA})}\right] \tag{45}$$

3) **Cooling strategy**

In the present work we used a cooling scheme of

$$T_{SA} = T_{SA0}.q^m \tag{46}$$

The initial temperature T_{SA0} is of major importance. Overvaluing would lead to high computational effort without any benefit because almost every new state is going to be accepted. In the case of an undervalued T_{SA0} the walker might be trapped in a local minimum.

The tunable parameters q, m, σ_i as well as the initial values for x_i used for the calculations are documented in the results section. In the case that none of the states x_n had been

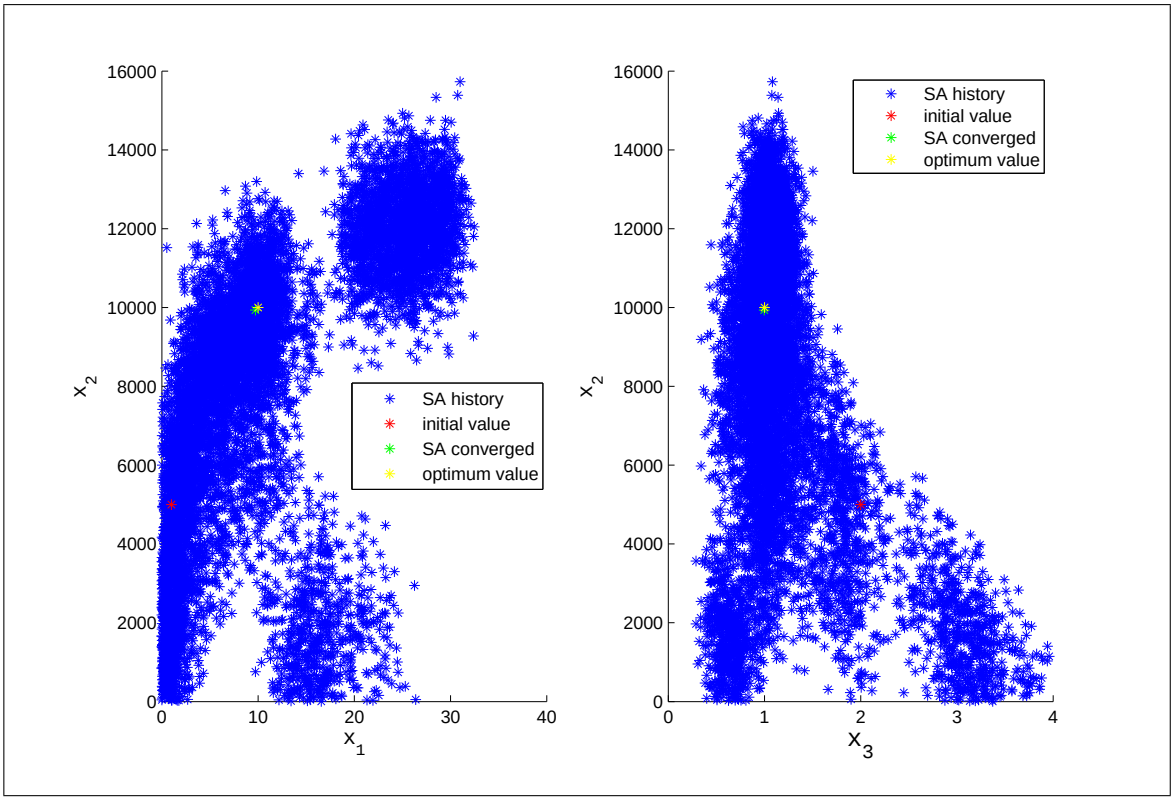

Figure 7: Summary of the simulated annealing algorithm for parameter estimation in our case study

accepted for 200 suggestions, the algorithm was assumed to have reached convergence. If the objective function was observed to be less during the computation at some other point in the parameter space, the latter one was updated as the new state.

3.2.2 Particle swarm optimization (PSO)

The algorithm was initially proposed by Kennedy and Eberhart (1995), as a methodology for the optimization of nonlinear functions. Various modifications have been made to the original algorithm by researchers in order to make the method more suitable for their system. Although, meta heuristic techniques (including PSO) take a very long time for its computation owing to the multiple function evaluations involved, these function evaluations can be later utilized for statistical analysis. The method tries to mimic the process of birds

flocking and is based on the swarming theory. In the case of the PSA a bird is an element

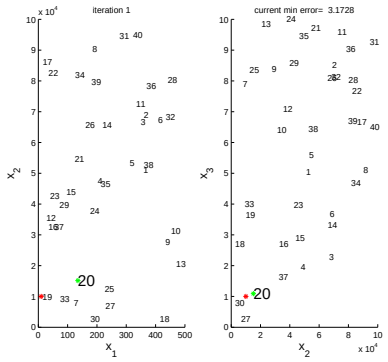

(a) Initial random distribution

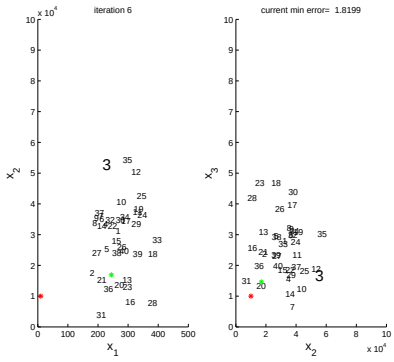

(b) Iteration 6: Birds begin to concentrate

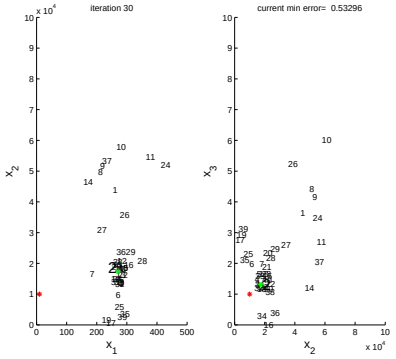

(c) Iteration 30: Concentration of the birds increase in the region around one point

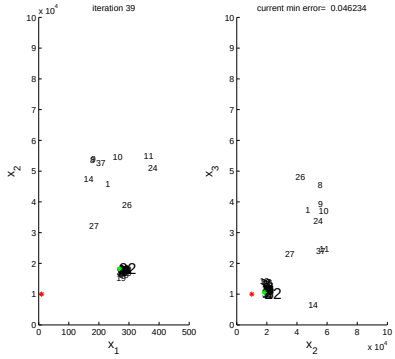

(d) Iteration 39: Birds found a promising point and concentrate around it

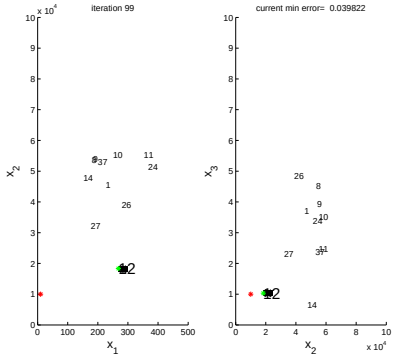

(e) Final Iteration: The promising point found by the birds get refined and most birds concentrate around it to form a 'focus'

Figure 8: Distribution of the "birds" over the entire domain showing the principle of the particle swarm algorithm

moving in the parameter space where it calculates the corresponding objective function. The algorithm is based on the synchrony of the flocking behavior and depends significantly on the inter-individual distances between the birds and their neighbors. The birds are set to "fly" in the search domain, i.e. the parameter space, according to the equations

$$v_b^{t+1} = w.v_b^t + c_1.rand_1.(b_{best} - x_b^t) + c_2.rand_2.(g_{best} - x_b^t) \tag{47}$$

$$x_b^{t+1} = x_b^t + v_b^{t+1}.\Delta t \tag{48}$$

Here b represents the bird, t is the number of iterations, v_b and x_b are the velocity and position of the bird respectively, c_1 and c_2 are called the cognitive and social parameters, w is the inertial weight which was an inclusion into the algorithm by Shi and Eberhart (1998), $rand_1$ and $rand_2$ are random numbers, b_{best} is the best known position x having the lowest objective function $\Phi(x)$ the bird itself and g_{best} is the best known position of the entire particle (bird) swarm.

Initially N birds were distributed randomly in the parameter space (see table 4), with a random initial velocity using a maximum value of a fourth of the parameter spaces elongation per time step ($\Delta t = 1$). Birds leaving the parameter were updated according to the "mirroring" concept in which the bird is mapped back into the parameter space with a sign inversion of its velocity. After each time step it was checked if some bird was able to improve his b_{best} or if g_{best} was being improved by the particle swarm. In our study, 20 birds were considered at each iteration and a maximum of 100 iterations were allowed. The striking characteristic of this algorithm is its aspect of having the birds spread all over in the search

domain during the initial iterations and then have the birds more concentrated to the regions which seems more promising. This way the algorithm tends to be more convergent towards the later iterations. An initial value like in the case of the SSA is not required.

3.2.3 gEST using gPROMS

The dynamic optimization algorithm implemented by PSE, UK with the gPROMS software is one of the finest technique existent in the present day optimization community. A flexibility to use the maximum likelihood function or the least square objective function is available in this parameter estimation platform. If is the measured variable $\hat{Y_{ijk}}$ and Y_{ijk} is the predicted variable, the maximum likelihood function can be defined as

$$\phi(k,\theta) = \frac{M}{2}.\ln(2\pi) + \frac{1}{2}.\min\left\{\sum_{i=1}^{a}\sum_{j=1}^{b_i}\sum_{k=1}^{c_{i,j}}\left[\ln(\sigma_{ijk}^2) + \frac{(\hat{Y_{ijk}} - Y_{ijk})^2}{\sigma_{ijk}^2}\right]\right\} \tag{49}$$

Where M is the total number of measurements taken during all experiments $a, b_i, c_{i,j}$ are the number of experiments, number of variables in the ith variable and number of measurements in the ith experiment of the jth variable respectively. σ_{ijk} is the variance of the kth measurement of the jth variable in the ith experiment and can be defined by many variance models such as a homoscedastic (constant variance) or a heteroscedastic model (variance is a function of the measured and the predicted values). In case of the homoscedastic variance model, the maximum likelihood function is simplified to a weighted least square form whereas when a purely heteroscedastic model is chosen, the maximum likelihood objective function takes a more complicated form with the variance, σ as a function of the measured value raised to a parameter γ (which lies between 0 and 1). The two

asymptotic conditions of the parameter, γ leads to the constant variance ($\gamma = 0$) and the constant relative variance ($\gamma = 1$) cases.

Using the gEST parameter estimation algorithm available with the gPROMS platform, any of the above mentioned variance models can be chosen and the other parameters can also be specified by the user. However, we have used the homoscedastic models with constant or constant variance models in this work. Since our measured/known quantity is generated through simulations, the data is devoid of much variance, thus making it affordable to choose a more simplistic variance model for accurate estimation.

3.3 Quality criterion

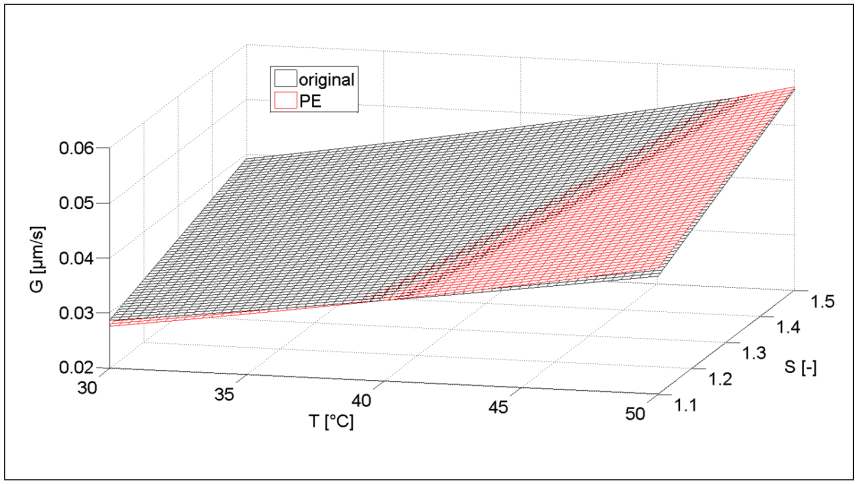

Figure 9: One value quality criteria of the PE output (PSA Exp1+3)

In the present work we introduce the one value quality criteria to evaluate and compare the PE outputs of the different algorithms. To quantify the difference between the real growth rate and the one obtained by substituting the parameters obtained by the PE into the growth rate expression, we calculated the differences in a parameter space of temperature and super supersaturation typically for the performed crystallization experiments/simulations.

We defined the one value quality criteria Q_{PE} as follows:

$$Q_{PE} = \int_{1.1}^{1.5} \int_{30}^{50} |G_{original} - G_{PE}| \; dT[^0C] \; S[-] \tag{50}$$

4 Materials and methods for experimental studies

Some experimental studies were also conducted using the fluid bed equipment manufactured by Innojet technologies. The nozzle used for the spraying of $liquid/liquid + binder$ was the Innojet annular gap spray nozzle Rotojet type IRN 2 with $2mm$ annular gap diameter, 6.28 mm developed length, 0.25 mm gap width, 1.57 mm^2 free spraying cross-section and 2.09 nl/s air consumption at 1 bar spraying pressure. The material used for the study was a mixture of 0.82 fraction of Lactose ($350gms$) and 0.18 fraction of Starch ($75gms$). The binder material used for granulation was Kollidon 25 with which a 0.15 mass fraction solution was prepared. The batch size containing the solid material was 425 gms.

Control and operation of fluid bed equipment for granulation is more challenging owing to the multiple operating parameters than affect the process. Different fluid bed granulation systems require different set of variables. Important factors that affect the fluid bed granulation process can be divided into two distinct groups which are equipment related variables and process related variables. The former includes 1)pressure drop and 2)filter shaking. The latter includes 1) inlet air temperature, 2) nozzle atomization pressure, 3) fluidization air velocity and 4)nozzle position. It has been identified that the cardinal parameters than need to be controlled for efficient operation of the equipment is the product temperature, flow rate of air, spray rate of the liquid, total liquid to solid ratio (L/S)and concentration of the binder (Kollidon) in the solution. The total L/S ratio was manipulated by changing the time span over which the equipment was operated for a specific flow rate. A DOE was prepared for detailed analysis of the various operating parameters on the final outcome of the granulation process using a fluid bed equipment. The base case for the study was considered having the

Figure 10: Front view of the fluid bed equipment as in the laboratory

conditions: spray rate of the liquid=7gm/min, L/S=0.2, product temperature=35^0C, air flowrate=34 m^3/min, concentration of Kollidon in the spraying solution=15 % and atomizing pressure=1 bar. For this case, the granulation equipment had to be operated for 12.14 mins. Using this base case, various scenarios were run on the equipment with a high, low and base case for each cardinal operating parameter affecting the granulation outcome. Table 3

summarizes the various values for the operating parameters chosen for this study. For each scenario, only one parameter was manipulated and all the others were held constant as per the values for the base case.

Table 3: Design of experiments for the experimental study

Parameter name	**High**	**Base**	**Low**
Liquid Spray rate (gm/min)	10	7	4
Total liquid to solid ratio (%)	25	20	15
Total time of operation ($mins$)	15.18	12.14	9.1
Product temperature (^0C)	40	35	30
Air flow rate (m^3/min)	40	34	28
Concentration of Kollidon 25 (%)	25	15	0

5 Numerical Techniques for solution of the 3-D PBM

Besides the model development, employing an appropriate numerical technique for solution to such hyperbolic integro-partial differential equation is yet another common challenge. Various complexities are faced with the solution of the multidimensional PBM due to the presence of multiple time scales and multiple dimensions. Therefore developing robust models with efficient solution techniques for such a framework is a crucial task.

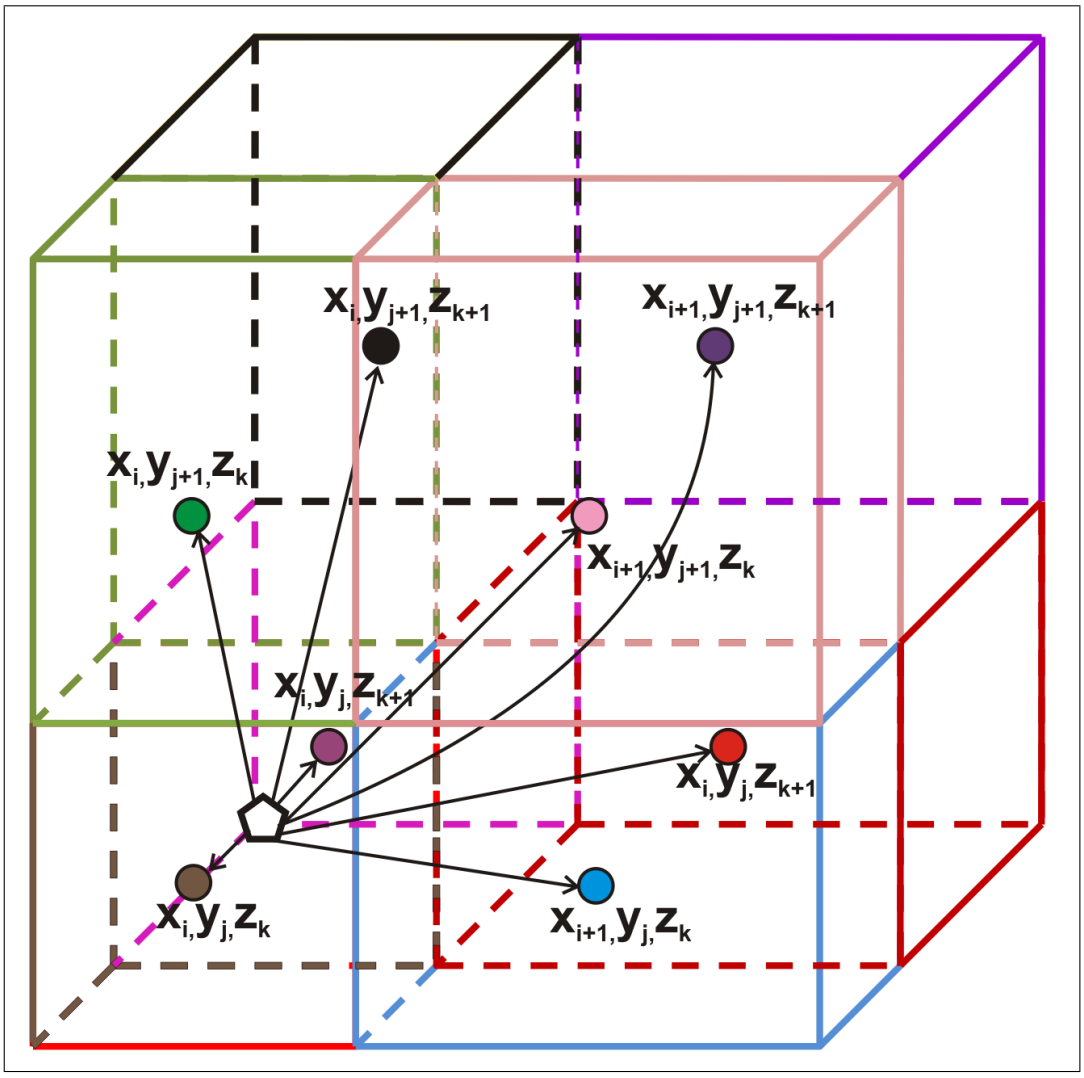

Figure 11: Discretized non-linear grid in three dimensions

The partial derivatives with respect to the internal coordinates representing the various underlying mechanisms are addressed using finite volumes. In order to span a broader size

range, a non-linear grid has been used for the discretization followed by the cell average technique (Kumar et al., 2006) for the solution. Due to the non-linear grid, the newly formed particles in aggregation and breakage mechanism do not exactly fall on the representative volume for the discretized grid. Significant developments have been made in promoting the use of cell average techniques. Kumar and Ramkrishna (1996b,a) led to the proposal of the fixed-pivot discretization technique (FPDM) and moving pivot discretization technique which could be used to allocate particles to the neighbouring grids when the daughter particle did not exactly fall on the pivot in a non-linear grid. Later Chakraborty and Kumar (2007) extended this approach for higher dimensional formulations. This technique by Kumar and Ramkrishna (1996b) was quite efficient but was accompanied by over-prediction of particle property distribution. The shortcomings from this technique was alleviated to a great extent by the cell-average technique proposed by Kumar et al. (2006, 2008). Both the Fixed Pivot and Cell Average Techniques distribute birth falling on non-representative points to the nearest representative points, with a certain fraction of the total birth going to each neighbouring representative points. The Fixed Pivot technique distributes the births as they occur. The Cell Average Technique, on the other hand, performs a local-averaging for each cell (at each time step) before distributing it to the adjoining representative points for a nonlinear, arbitrary grid. This justifies the implementation of cell average technique for the purpose of solution of our PBM. Thus a new set of fractionation equations are required in order to reassign the newly formed particles to the adjoining bins such that the volume/mass is conserved along with other lower moments. In our previous works, we have dealt with obtaining the fractionation equations for the reassignment of particles (during aggregation and breakage) for the non-linear grid, based on the cell average technique. The

result is an ODE with respect to time wherein the growth terms, the source terms and the circulation terms (between the two compartments) are in the form of algebraic equations. This final ODE (IVP) is integrated using the first order Euler technique. Equation (1) can be expressed in the discrete form as shown in Equations (51) and (52)

$$\frac{dF'_{1,i,j,k}}{dt} + \left(\frac{F'_{1,i,j,k}}{\triangle s_i} \frac{ds}{dt}\Big|_{s_i} - \frac{F'_{1,i+1,j,k}}{\triangle s_{i+1}} \frac{ds}{dt}\Big|_{s_{i+1}} \right) + \left(\frac{F'_{1,i,j,k}}{\triangle l_j} \frac{dl}{dt}\Big|_{l_j} - \frac{F'_{1,i,j+1,k}}{\triangle l_{j+1}} \frac{dl}{dt}\Big|_{l_{j+1}} \right)$$
$$+ \left(\frac{F'_{1,i,j,k}}{\triangle g_k} \frac{dg}{dt}\Big|_{g_k} - \frac{F'_{1,i,j,k+1}}{\triangle g_{k+1}} \frac{dg}{dt}\Big|_{g_{k+1}} \right) = \Re_{agg}(s_i, l_j, g_k) + \Re_{break}(s_i, l_j, g_k) - a \left(\frac{F_{1,i,j,k}}{1-\alpha} - \frac{F_{2,i,j,k}}{\alpha} \right) \quad (51)$$

$$\frac{dF'_{2,i,j,k}}{dt} + \left(\frac{F'_{2,i,j,k}}{\triangle s_i} \frac{ds}{dt}\Big|_{s_i} - \frac{F'_{2,i+1,j,k}}{\triangle s_{i+1}} \frac{ds}{dt}\Big|_{s_{i+1}} \right) + \left(\frac{F'_{2,i,j,k}}{\triangle l_j} \frac{dl}{dt}\Big|_{l_j} - \frac{F'_{2,i,j+1,k}}{\triangle l_{j+1}} \frac{dl}{dt}\Big|_{l_{j+1}} \right)$$
$$+ \left(\frac{F'_{2,i,j,k}}{\triangle g_k} \frac{dg}{dt}\Big|_{g_k} - \frac{F'_{2,i,j,k+1}}{\triangle g_{k+1}} \frac{dg}{dt}\Big|_{g_{k+1}} \right) = \Re_{agg}(s_i, l_j, g_k) + \Re_{break}(s_i, l_j, g_k) + a \left(\frac{F_{1,i,j,k}}{1-\alpha} - \frac{F_{2,i,j,k}}{\alpha} \right) \quad (52)$$

Here $F'_{i,j,k} = \int_{s_i}^{s_{i+1}} \int_{l_j}^{l_{j+1}} \int_{g_k}^{g_{k+1}} F(s,l,g)\, ds\, dl\, dg$, s_i is the value of the solid volume at the upper end of the i^{th} bin along the solid volume axis, l_j is the value of the liquid volume at the upper end of the j^{th} bin along the liquid volume axis, g_k is the value of the gas volume at the upper end of the k^{th} bin along the gas volume axis. $\triangle s_i$, $\triangle l_j$ and $\triangle g_k$ are the sizes of the i^{th}, j^{th} and k^{th} bin with respect to the solid, liquid and gas volume axis. Using this technique, the population balance equation, is reduced to a system of ordinary differential equations in terms of the aggregation ($\Re_{agg}(s_i, l_j, g_k)$) and breakage ($\Re_{break}(s_i, l_j, g_k)$). The triple integral for the aggregation term can thereby be evaluated by casting it into simpler addition and multiplication terms. Assuming that the

particle fractions $a_1, a_2, a_3, a_4, a_5, a_6, a_7,$ and a_8 are distributed to the neighbouring nodes $P_{i,j,k}, P_{i,j+1,k}, P_{i+1,j+1,k}, P_{i,j+1,k},\ P_{i,j,k+1}, P_{i,j+1,k+1}, P_{i+1,j+1,k+1}, and P_{i,j+1,k+1}$, respectively, the fractionation equations thus obtained from our previous works can be expressed as Equations (53)-(60)

$$a_1 = \frac{(x_{i+1} - \bar{x}_i)(y_{j+1} - \bar{y}_j)(z_{k+1} - \bar{z}_k)}{(x_{i+1} - x_i)(y_{j+1} - y_j)(z_{k+1} - z_k)} B_{ijk} \tag{53}$$

$$a_2 = \frac{(\bar{x}_i - x_i)(y_{j+1} - \bar{y}_j)(z_{k+1} - \bar{z}_k)}{(x_{i+1} - x_i)(y_{j+1} - y_j)(z_{k+1} - z_k)} B_{ijk} \tag{54}$$

$$a_3 = \frac{(\bar{x}_i - x_i)(\bar{y}_j - y_j)(z_{k+1} - \bar{z}_k)}{(x_{i+1} - x_i)(y_{j+1} - y_j)(z_{k+1} - z_k)} B_{ijk} \tag{55}$$

$$a_4 = \frac{(x_{i+1} - \bar{x}_i)(\bar{y}_j - y_j)(z_{k+1} - \bar{z}_k)}{(x_{i+1} - x_i)(y_{j+1} - y_j)(z_{k+1} - z_k)} B_{ijk} \tag{56}$$

$$a_5 = \frac{(x_{i+1} - \bar{x}_i)(y_{j+1} - \bar{y}_j)(\bar{z}_k - z_k)}{(x_{i+1} - x_i)(y_{j+1} - y_j)(z_{k+1} - z_k)} B_{ijk} \tag{57}$$

$$a_6 = \frac{(\bar{x}_i - x_i)(y_{j+1} - \bar{y}_j)(\bar{z}_k - z_k)}{(x_{i+1} - x_i)(y_{j+1} - y_j)(z_{k+1} - z_k)} B_{ijk} \tag{58}$$

$$a_7 = \frac{(\bar{x}_i - x_i)(\bar{y}_j - y_j)(\bar{z}_k - z_k)}{(x_{i+1} - x_i)(y_{j+1} - y_j)(z_{k+1} - z_k)} B_{ijk} \tag{59}$$

$$a_8 = \frac{(x_{i+1} - \bar{x}_i)(\bar{y}_j - y_j)(\bar{z}_k - z_k)}{(x_{i+1} - x_i)(y_{j+1} - y_j)(z_{k+1} - z_k)} B_{ijk} \tag{60}$$

These fractions were obtained from conservation equations ensuring the volume was constant after the reassignment. These conservation equations can be written as

Then, the particle fractions must satisfy the following thirteen equations, to conserve the total volume as well as the particle number.

$$B_{ijk} = a_1 + a_2 + a_3 + a_4 + a_5 + a_6 + a_7 + a_8 \tag{61}$$

$$a_1 x_i + a_2 x_{i+1} = (a_1 + a_2)\bar{x}_i \tag{62}$$

$$a_3 x_{i+1} + a_4 x_i = (a_3 + a_4)\bar{x}_i \tag{63}$$

$$a_5 x_i + a_6 x_{i+1} = (a_5 + a_6)\bar{x}_i \tag{64}$$

$$a_7 x_{i+1} + a_8 x_i = (a_7 + a_8)\bar{x}_i \tag{65}$$

$$a_1 y_j + a_4 y_{j+1} = (a_1 + a_4)\bar{y}_j \tag{66}$$

$$a_2 y_j + a_3 y_{j+1} = (a_2 + a_3)\bar{y}_j \tag{67}$$

$$a_5 y_j + a_8 y_{j+1} = (a_5 + a_8)\bar{y}_j \tag{68}$$

$$a_6 y_j + a_7 y_{j+1} = (a_6 + a_7)\bar{y}_j \tag{69}$$

$$a_1 z_k + a_5 z_{k+1} = (a_1 + a_5)\bar{z}_k \tag{70}$$

$$a_2 z_k + a_6 z_{k+1} = (a_2 + a_6)\bar{z}_k \tag{71}$$

$$a_3 z_k + a_7 z_{k+1} = (a_3 + a_7)\bar{z}_k \tag{72}$$

$$a_4 z_k + a_8 z_{k+1} = (a_4 + a_8)\bar{z}_k \tag{73}$$

Using the abovementioned approach, the numerical steps have been hardcoded in MATLAB (version 2012a) in order to solve the PBE using a robust technique. The same approach is also used for solving the 1-D PBM for crystallization. The mechanistic kernels for aggregation and breakage have also been coded in separate function files, where the modified values for the quantities such as external surface liquid and reduction in porosity have been updated instantaneously at each time step. The simultions were run on a machine with quad-core Intel Corei7-870 CPU (2.93 GHz) processor and 8 GB RAM running Windows 7 (64 bit) OS. The stability of the numerical technique was ensured (while using the explicit

Euler technique) by making an appropriate choice for the grid sizes and time steps, such that the CFL conditions were not violated.

6 Results and Discussion

Intuitively we have identified a few parameters that could be easily manipulated while running experiments in order to obtain a detailed sensitivity analysis of the proposed integrated model that is expressed as a function of the key operating parameters. This study will enable us to have a more vivid idea of which quantities are needed to be manipulated and to what extent, when a certain final outcome is desired. The integrated model relates the various mechanisms to the fundamental operating parameters in a way such that the model is not completely decoupled, yet the solution technique is not very complicated. The interaction between the various mechanisms such as consolidation and aggregation, with each other, can be be addressed with the approach proposed in this paper. Some of the crucial operating parameters that affect the final outcome of the process are the number of rotations per minute of the impeller (rpm), the viscosity of the binder (μ), the contact angle (θ) of the binder liquid onto the surface of the particle and the liquid spray rate. The aggregation kernel proposed in this work is also quite novel and takes into affect the various crucial operating parameters such as the viscosity of binder, contact angle and impeller speed.

6.1 Comparison between the semi-mechanistic aggregation and the empirical kernels from literature

The aggregation kernel proposed in this paper, and taken into account for our simulations, is dynamic in nature such that the kernel can be updated along with the changes in the system behavior. The aggregation kernel takes into account the appearance of surface liquid for porous particles as liquid is sprayed over the particles with the progress of the granulation

process. The amount of wetted area is also represented as a function of the contact angle and the Stoke's criterion takes into account the viscosity effects. The overall aggregation kernel is expressed as a product of the fractional wetted area, the factor owing to the Stoke's criterion, the size dependant part represented by the kernel proposed by Madec et al. (2003) and the constant value for scaling the kernel. In contrast to the empirical kernels more commonly used, this kernel shows remarkable variations with respect to the different internal coordinates, such as solid, liquid and gas volumes. Also, at the initial time, the particles that are more porous and dry are considered to not have any aggregating tendency. These trends cannot be captured using the empirical kernels. Figure 12 shows a comparison between the empirical kernels and the kernel proposed in this work.

From Fig 12, we can see that for the empirical kernel, the individual volumes are just lumped as the size and hence there is no realistic variation with respect to the individual volumes. The semi-mechanistic kernel instead, shows more realistic variation with respect to the solid, liquid and gas volumes. The kernel comprises of a size dependant and a size independent portion. The size independent portion has been shown in Fig 12c where the true behavior can be captured. For a constant solid and gas volume, as the liquid increases, the fractional wetted area also increases, which is in agreement with the figure. On the other hand, for a constant solid and liquid volume, the wetted area decreases as the porosity increases. As the porosity increases, a significant amount of liquid is used up to fill in the pores of the particle and after a certain point, surface liquid seems to emerge. Thus the amount of surface liquid and thus the wetted area is reduced for highly porous particles. For a constant liquid and gas volume, the fractional wetted area decreases as the solid volume increases. Due to increased solid volume, the overall size of the particle increases, but the

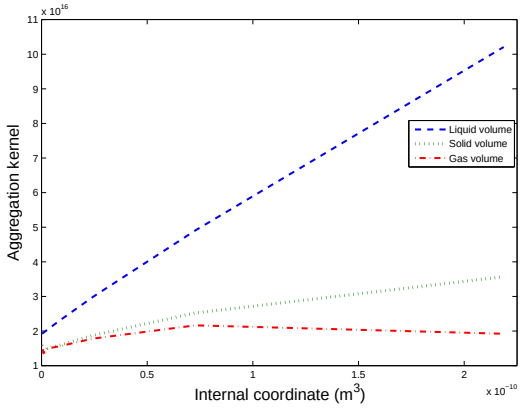

(a) Semi-mechanistic kernel

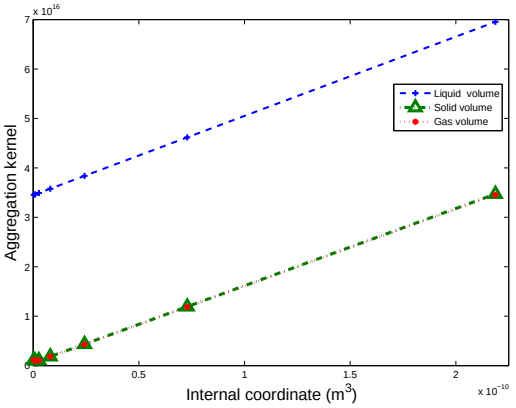

(b) Empirical kernel

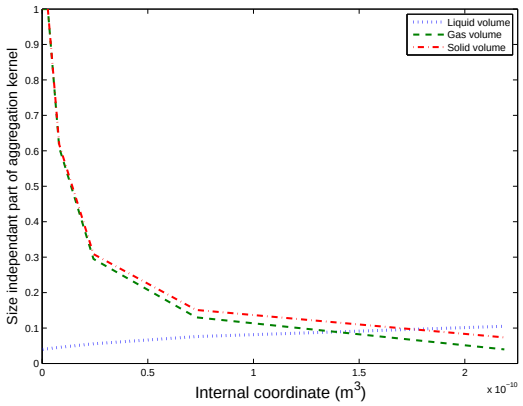

(c) Size independant portion of the semi-mechanistic kernel

Figure 12: Comparison of the behavior of the semi-mechanistic kernel and the empirical kernels with respect to the individual volumes ($\beta(1,1,1,1,1,:)$ *for gas*, $\beta(1,1,1,1,:,7)$ *for liquid and* $\beta(1,1,1,:,1,1)$ *for solid in both cases*)

liquid amount is still constant hence the amount of wetted area is same, but the total surface area present in the denominator is increased and hence the fractional wetted area is reduced. These physical events can be well captured in the aggregation kernel proposed by us.

6.2 Dynamic sensitivity analysis of the model inputs/operating parameters

A dynamic sensitivity analysis has been showcased in this section which highlights the pros and cons of considering this integrated model and the ability for it to capture the system behavior that is observed in realistic scenarios. The integrated model which also takes into account the various fundamental operating parameters, can capture the steady growth and induction behavior under the conditions as also mentioned in the works of Walker (2007). This suggests the effectiveness of the model to be able to predict realistic scenarios and could be extended for control and optimization purposes. As already mentioned, the crucial operating parameters that have been taken into consideration are viscosity of the binder, contact angle of the binder on the particle surface, the amount of liquid added and the speed of the impeller. The impeller speed affects both the aggregation and the consolidation of the particles, the viscosity and contact angle affect both the aggregation and the breakage mechanisms, the liquid added affects the aggregation and the liquid distribution. The compartmental based model gives a more realistic picture of the system due to the inhomogeneity associated with the binder distribution. Although, consideration of two compartments is not a very accurate representation, but this approach can be implemented with multiple compartments thus obtaining a more realistic picture. The dynamic sensitivity analysis can be broadly classified into the steady state case and the induction behavior.

Steady state growth

The steady state behavior was noticed for a system having higher aggregation, lower consolidation, higher binder liquid addition and low porosity of the initial particles. The parametric values used for the base case of the steady state behavior has been listed in the table 4.

Table 4: Parametric values for the simulations in the steady state case

Parameter name	**Value**
ρ_{solid}	2500 kg/m^3
ρ_{liquid}	1000 kg/m^3
ρ_{gas}	1 kg/m^3
Number of grids in solid, liquid and gas volume	7
Grid width of the i^{th} bin (same in each volume)	$(3 \times 10^{-13}) \times 3^i$ m^3
Initial mass charged to the granulation, $F(1,1,1)$	0.2 kg
Binder Spray rate, u	0.5 ml/sec
c_{binder}	0.1
ϵ_{min}	0.2
Rpm of the impeller	220
Diameter of the impeller	$0.02m$
Consolidation constant, c	1×10^{-13}
Aggregation Constant for the kernel, b_0	2×10^{21}
Granule saturation at which surface liquid first appears, s^*	0.2
Viscosity μ	0.006 $kg/m - sec$
Liquid surface tension γ_{lv}	$0.0728 N/m^2$
Coefficient of restitution e	0.04
Surface asperity h_a	0.01 of $diameter$
Droplet diameter	70 μm
Constant contact angle of the liquid on the particle surface	$50^0 degrees$
Portion of the overall population enclosed in domain 1, α_1	0.3
Circulation rate between the two compartments	1×-27
Premixing time	120 $secs$
Liquid addition time	$120 - 300$ $secs$
Wet massing time	$300 - 400$ $secs$
Parameters specific to the breakage kernel were obtained from Ramachandran et al. (2009)	

Initially the particles are dry, but as liquid is added, a huge amount of aggregation begins to occur thus leading in the average diameter to shoot up. Also, since the consolidation of particles is lower, the particles are not hugely dependent on the liquid to be squeezed onto

the surface from inside the pores. This leads to a steady growth of particles due to the large aggregation tendency and the the liquid addition. We have studied the various cases, by changing the crucial parameters as mentioned before.

6.2.1 Viscosity variation

Figure 13 shows the variation of the bulk and distributed properties with respect to the viscosity of the binder liquid used. It can be intuitively said, that a higher viscosity will lead to higher aggregation as the binder liquid enhances sticking together of fine powder to form aggregates. A similar physics can also be observed in the aggregation kernel. The Stoke's criterion exhibits the effect of viscosity on the aggregation of particles. The viscous Stoke's number represented by equation (23) shows an inverse proportionality with the viscosity. Thus when the viscosity is higher, the Stoke's number is smaller and hence the variable representing the fractional wetted area of the particles, Ψ is less sparse (with more 1's compared to 0's). This enables more cases possible for aggregation thus leading to higher aggregation and increased particle size. From the figures, we can see that for the value of viscosity above the base viscosity that we have used for our simulations, there is no significant change in the particle diameter. Thus, it is safe to comment, that for a certain liquid sprayrate, beyond a certain viscosity, there is no significant increase in the particle size.

The variation in viscosity does not have a significant effect on the porosity of particles. There is some variation in the aggregation extent, but the influence on the porosity of particles does not seem significant. Also, there is a higher content of bigger particles as the viscosity is higher due to the formation of more aggregates. Also, it can be observed that

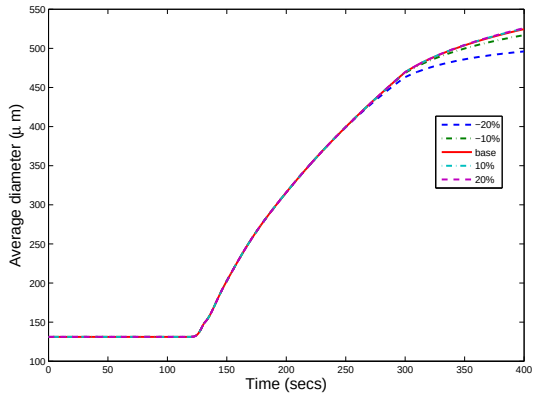

(a) Average diameter

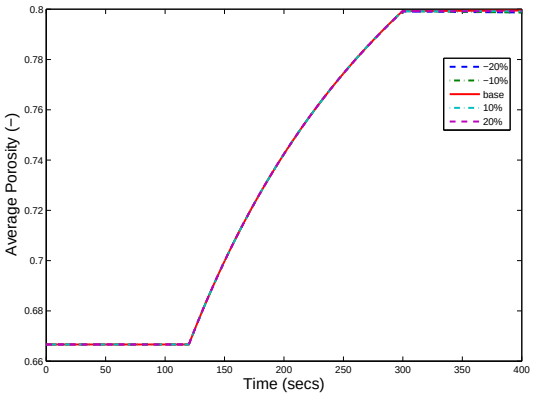

(b) Average porosity

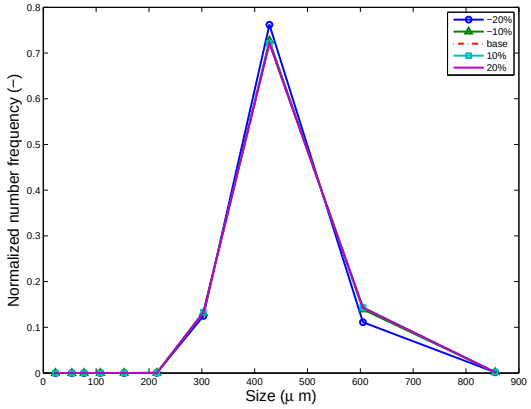

(c) PSD at the end of liquid addition

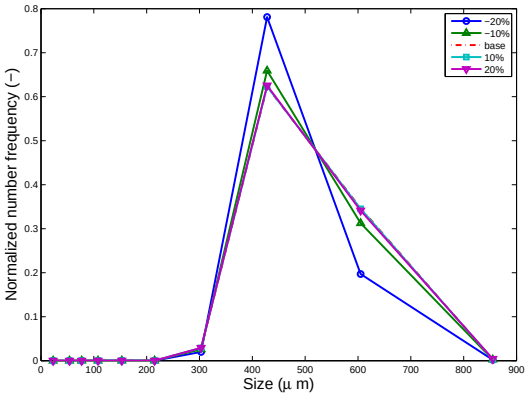

(d) PSD at the end of the wet massing time

Figure 13: Variation of viscosity for the steady growth process showing the effect on the bulk and distributed properties

the PSD at the beginning and end of the wet massing period are different.

6.2.2 Liquid amount variation

From figure 14, we see the affect of the liquid spray and the total amount of liquid on the average properties and the PSD at the end of liquid addition and wet massing time. It can also be qualitatively suggested that with higher liquid, the total volume of the particles increases, thus increasing the particle size and also with higher liquid addition, the number

of droplets formed are higher (as the volume of each droplet is constant) due to which each particle has a higher probability of being hit by a liquid droplet. Hence, the surface liquid available is higher and the aggregation kernel is raised. This also leads to an increase in the average size of the particles. The porosity of the particles are defined as the ratio of the liquid+gas volume to the overall particle volume. So, we can imagine that the amount of liquid directly affects the porosity of particles. Therefore, with increased liquid amount, the particle size and porosity increases and also, there is a slight shift in the PSD towards the right, indicating higher fraction of particles in the larger volume grids.

6.2.3 Impeller speed variation

Impeller speed has a significant effect on the aggregation, breakage and consolidation of particles. The affect of impeller speed is a bit more complicated than the previous subsections. We can see how the bulk and distributed properties are affected by the impeller speed in Figure 15. It can be noticed in the figure as well, that the effect of impeller speed is not very straightforward. Due to increased impeller speed, the breakage and consolidation of particles is higher due to higher collisions between particles. The particles tend to have more collisions but due to higher kinetic energy of the particles they impact more strongly against each other, thus leading to more breakage. There is some increase in the aggregation as well but the overall outcome is a reduction in the diameter increase. From equation (11) we can see that the consolidation rate has been expressed as a weak exponential function of the impeller speed. So, with higher impeller speed, the consolidation of particles is increased. Since, in the steady state case, the consolidation rate is not very high, so inspite of the fact that the consolidation of particles is increased, the effect on the average porosity of particles

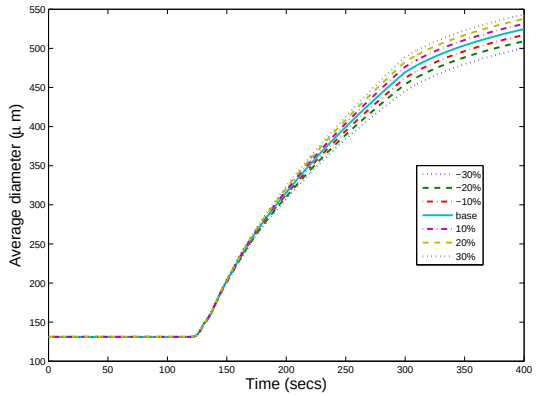

(a) Average diameter

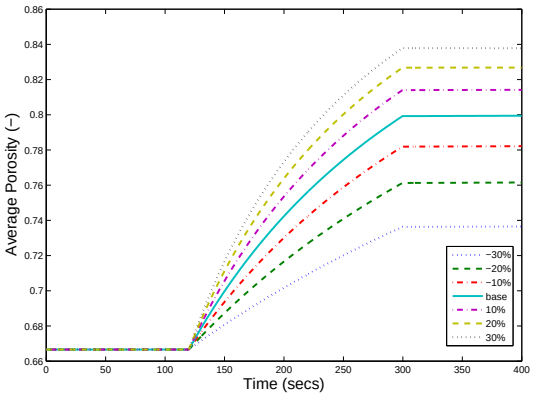

(b) Average porosity

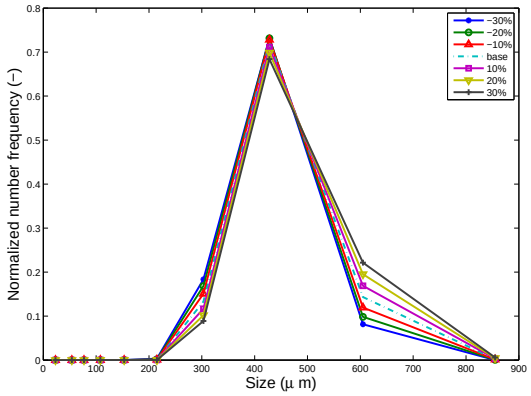

(c) PSD at the end of liquid addition

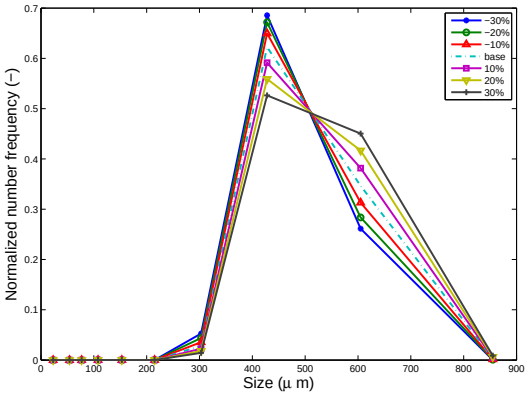

(d) PSD at the end of the wet massing time

Figure 14: Variation of amount of liquid for the steady growth process showing the effect on the bulk and distributed properties

is not very significant. Also the PSD of the particles seems to shift to the left for higher impeller speed at the beginning of the wet massing period. At the end of the wet massing period, there seems to be a higher fraction of smaller particles with increased impeller speed. This is inkeeping with the observations for the bulk properties of the particles.

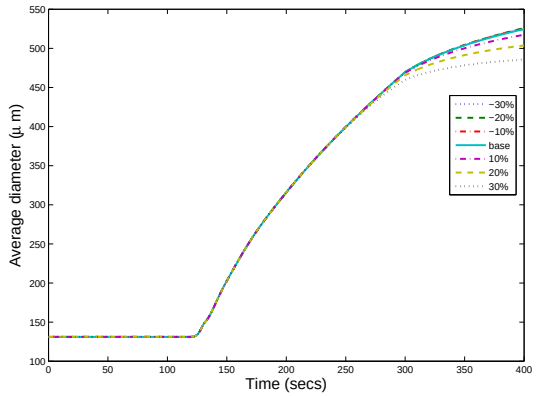

(a) Average diameter

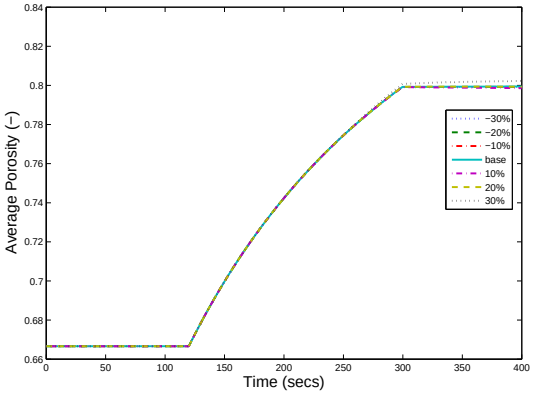

(b) Average porosity

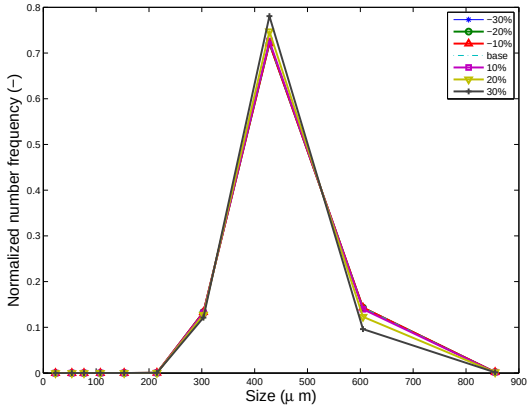

(c) PSD at the end of liquid addition

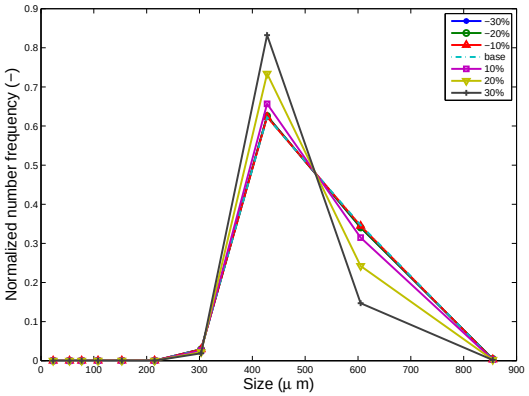

(d) PSD at the end of the wet massing time

Figure 15: Variation of impeller speed for the steady growth process showing the effect on the bulk and distributed properties

6.2.4 Contact angle variation

The contact angle of the binder liquid on the surface of the particle has a prominent influence on the aggregation and breakage of the particles. A major influence of the contact angle is on the fractional wetted area of the particles. The contact angle of the liquid on the solid surface suggests the wettability of the particle with the binder liquid used. Smaller contact angles suggest higher wettability and the converse is true for higher contact angles.

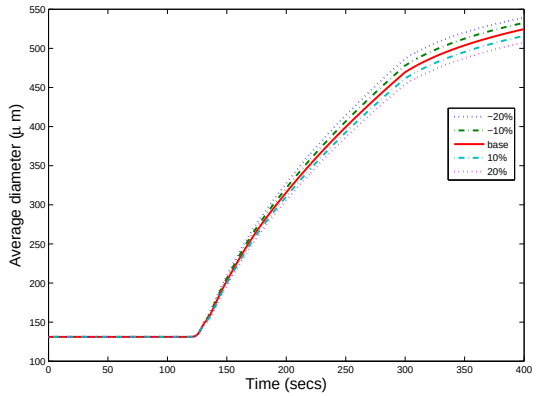

(a) Average diameter

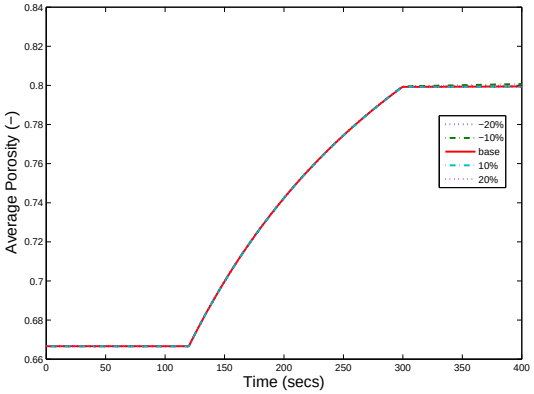

(b) Average porosity

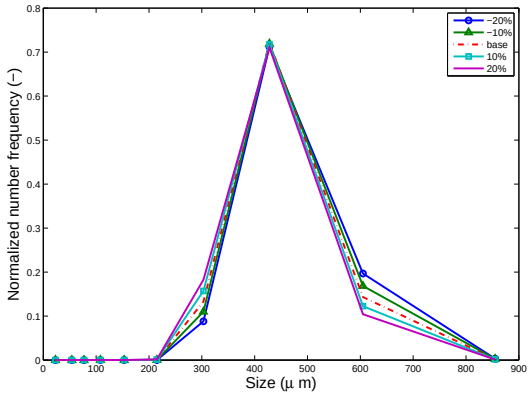

(c) PSD at the end of liquid addition

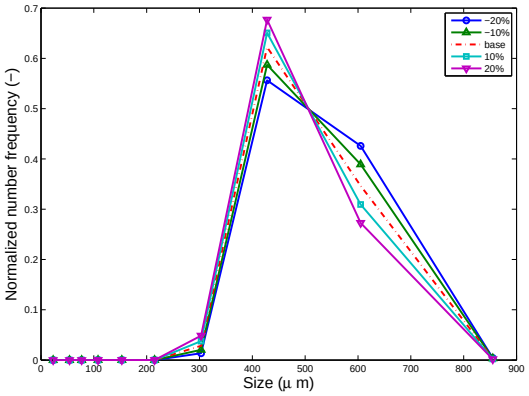

(d) PSD at the end of the wet massing time

Figure 16: Variation of contact angle between the binder liquid and the particle surface for the steady growth process showing the effect on the bulk and distributed properties

Values for contact angles over 90^0 degrees indicates hydrophobicity of the surface when water is used as the liquid. In our study, we have considered the contact angle to be such that the entire domain of study is within the hydrophillic/wettable range. Lower contact angle suggests a stronger liquid bridge between the two particles as seen in Equation (39) in the work by Ramachandran et al. (2009). Thus, the intrinsic strength of the particles is higher and it is more difficult to break the particles. With lower contact angles, the wettability characteristics of the particle is also better. Thus, the wetted surface area of

the particles is larger which also suggests a fractional wetted area of the particle closer to 1. This enhances the coalescence tendency of the particle as more area is available that allows colliding particles to stick to each other and aggregate. This behavior is also seen in Figure 16. The contact angle does not have an appreciable effect on the porosity of the particles. There is some increase in aggregation, thus leading to a slightly higher porosity, but the change in the average porosity is not very prominent. The PSD of the particle at the beginning and end of the wet massing period show good agreement with the bulk property plots. There is a higher fraction of bigger particles for a smaller contact angle.

Induction growth

The induction behavior can be realized for a system having relatively lower aggregation and higher consolidation such that enlargement of particles does not take place at the instant liquid is added to the surface. The values for the model parameters have been enlisted in the Table 5.

We have studied the induction behavior for two cases-porous primary particles and less porous primary particles. For the initial dry particles, there is a dearth in the surface liquid and hence very less aggregation occurs. As consolidation proceeds, the particles are compacted with reduced pore volume. This way, liquid is squeezed onto the surface of the particle thus leading to the availability of liquid on the surface for the coalescence. Therefore, there is a more gradual growth in the beginning but once the particles are enough wet, they grow steadily. A similar study has been performed for the induction behavior of the particles by varying the crucial operating parameters-viscosity of the binder liquid, amount and spray rate of liquid added, impeller speed and the contact angle of the binder liquid on the surface

Table 5: Parametric values for the simulations in the induction case

Parameter name	**Value**
ρ_{solid}	2500 kg/m^3
ρ_{liquid}	1000 kg/m^3
ρ_{gas}	1 kg/m^3
Number of grids in solid, liquid and gas volume	7
Grid width of the i^{th} bin (same in each volume)	$(3 \times 10^{-13}) \times 3^i$ m^3
Initial mass charged to the granulation, $F(1,1,1)$	0.2 kg
Binder Spray rate, u	0.5 ml/sec
c_{binder}	0.1
ϵ_{min}	0.2
Rpm of the impeller	220
Diameter of the impeller	$0.02m$
Consolidation constant, c	4×10^{-7}
Aggregation Constant for the kernel, b_0	7×10^{19}
Granule saturation at which surface liquid first appears, s^*	0.2
Viscosity μ	0.006 $kg/m - sec$
Liquid surface tension γ_{lv}	$0.0728N/m^2$
Coefficient of restitution e	0.04
Surface asperity h_a	0.01 of $diameter$
Droplet diameter	70 μm
Constant contact angle of the liquid on the particle surface	$50^0 degrees$
Portion of the overall population enclosed in domain 1, α_1	0.3
Circulation rate between the two compartments	1×-27
Premixing time	120 $secs$
Liquid addition time	$120 - 300$ $secs$
Wet massing time	$300 - 400$ $secs$
Parameters specific to the breakage kernel were obtained from Ramachandran et al. (2009)	

of the particle.

6.2.5 Viscosity variation

The effect of viscosity on the granulation of particles is similar for the induction behavior as that in the steady state behavior. The aggregation of particles is increased when the binder liquid is more viscous, as that facilitates the sticking of fine powder to each other. Thus, for more viscous liquid, the particles are a little larger. There is a slight difference in the

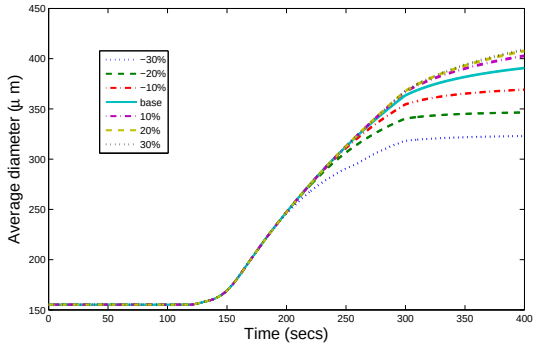

(a) Average diameter

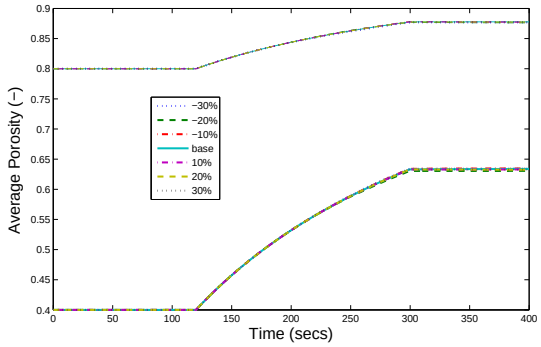

(b) Average porosity

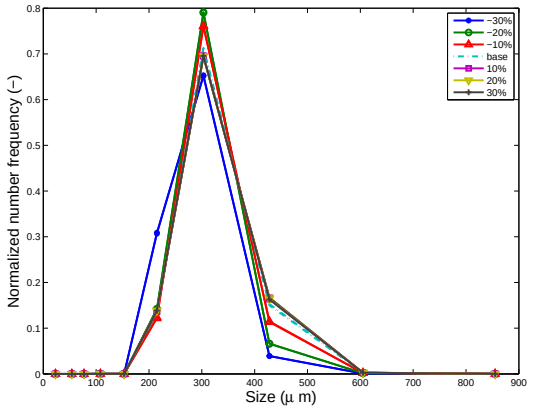

(c) PSD at the end of liquid addition

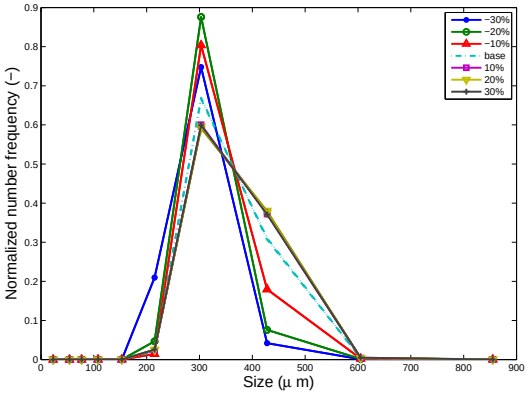

(d) PSD at the end of the wet massing time

Figure 17: Variation of viscosity for the induction behavior showing the effect on the bulk and distributed properties

average diameter and the PSD of the porous and the less porous particles due to the higher aggregation in case of the less porous particles. For analysis purpose, we have considered the two class of particles to have the same average diameter and moisture content, yet the less porous particles have higher solid content whereas the more porous particles have less solid content but higher gas volume. As we analyse the evolution of the particles over time, we see that the diameter of the particles are similar but the less porous particles have a slightly higher size, as the latter tends to suck more liquid as binder is added to it. Therefore the

availability of surface liquid on the porous particles is less than the non porous particles, leading to a lower rate of aggregation in case of the prior compared to the latter. Also, highly porous particles have a higher tendency of breaking, contributing to the reduced particle size of the population. The porosity of the porous primary particles consistently stays high relative to the less porous primary particles, even as the process of granulation proceeds. These trends are also revealed in Fig 13 which is able to capture the induction behavior of particle growth under the conditions observed in experimental practice.

6.2.6 Liquid amount variation

As also seen in the case for the steady state growth, the spray rate and the amount of liquid leads to an increase in the average diameter and the porosity of the particles. With increased liquid, not only is the particle volume increased, but also the availability of surface liquid is higher leading to higher aggregation of particles. The amount of liquid added in the induction case is less than that considered in the steady state case, inkeeping with the aggregation kernel used to exhibit the induction behavior. The porous particles tend to have a slightly smaller particle size due to the excessive pore volume which captures more liquid and leads to a reduced surface liquid availability on the particles suggesting reduced aggregation (Fig 18).

6.2.7 Impeller speed variation

With an increase in the rotational speed of the impeller, the kinetic energy of the particles is increased. This leads to a higher probability of collision but that involves a higher breakage rate of the particles. The compaction of particles in the form of consolidation is also higher

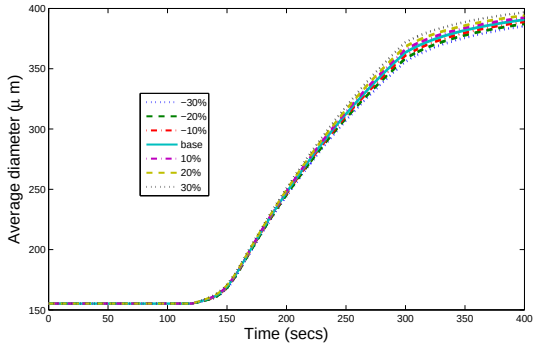

(a) Average diameter

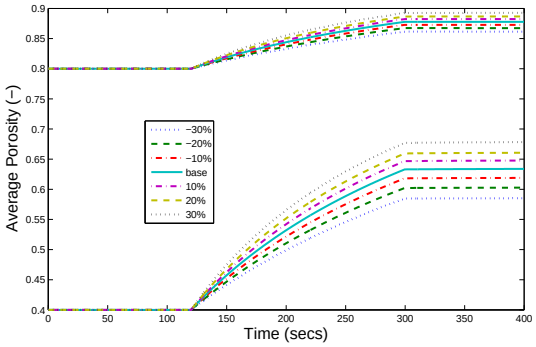

(b) Average porosity

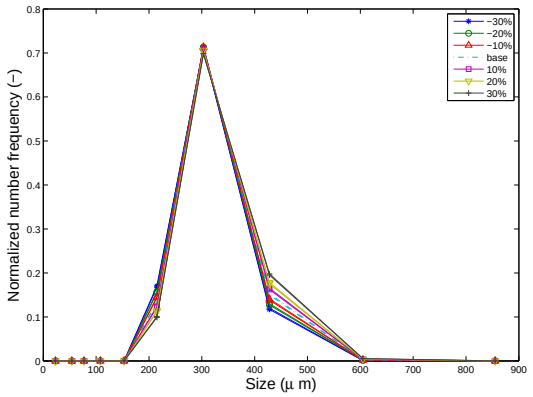

(c) PSD at the end of liquid addition

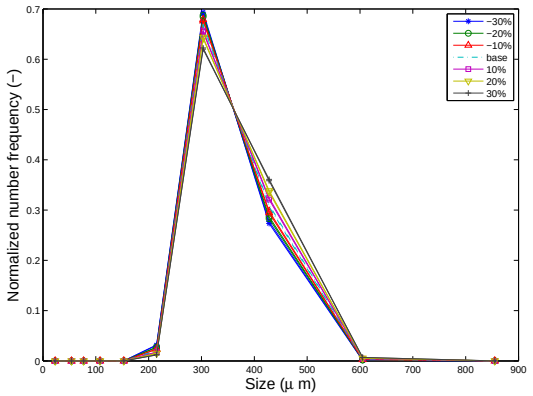

(d) PSD at the end of the wet massing time

Figure 18: Variation of amount of liquid for the induction behavior showing the effect on the bulk and distributed properties

when the impeller speed is increased. Thus from Fig 19, we can see that with a higher impeller speed, the particle size is reduced. This behavior has also been observed in case of the steady state growth. As also discussed before, there is a slight difference in the average diameter and particle size distribution of the porous and non porous particles due to the increased aggregation and reduced breakage in case of the latter compared to the prior.

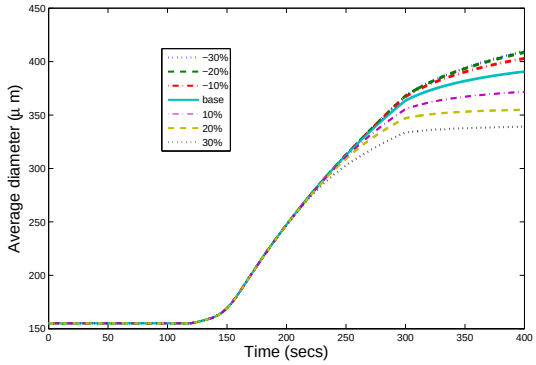

(a) Average diameter

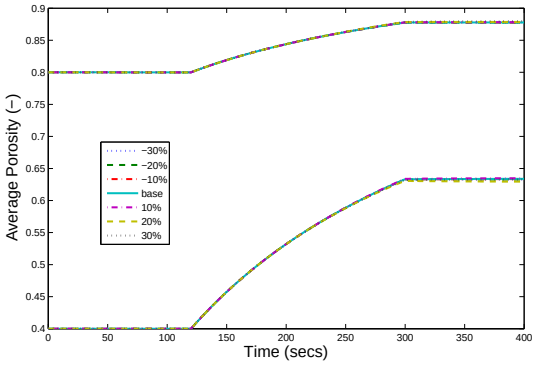

(b) Average porosity

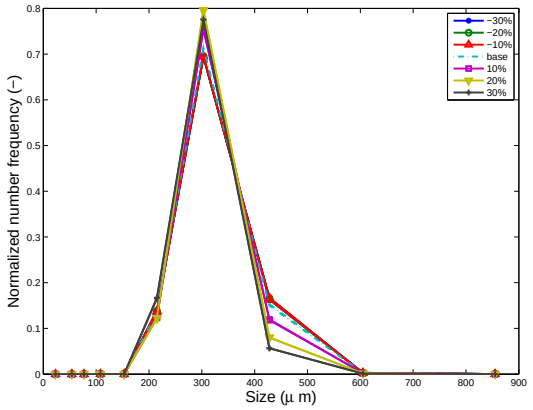

(c) PSD at the end of liquid addition

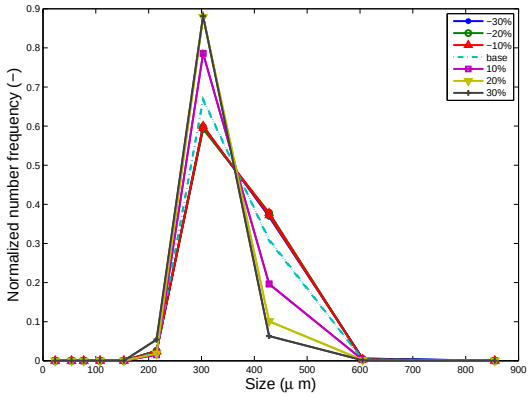

(d) PSD at the end of the wet massing time

Figure 19: Variation of impeller speed for the induction behavior showing the effect on the bulk and distributed properties

6.2.8 Contact angle variation

Fig 20 reveals the effect of contact angle variation on the bulk and distributed properties of a population which exhibits induction growth. As the particles are more hydrophilic suggesting a smaller contact angle, a higher surface coverage for the same amount of surface liquid is observed. This leads to a higher aggregation rate as the kernel has been proposed with a direct influence of the fractional wetted area on the aggregation rate. Thus, with reduced contact angle, the overall particle size of the population increases.

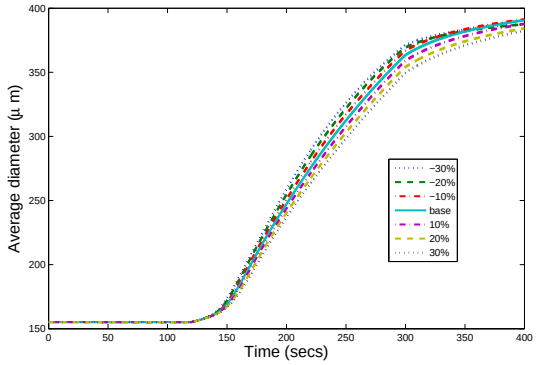

(a) Average diameter

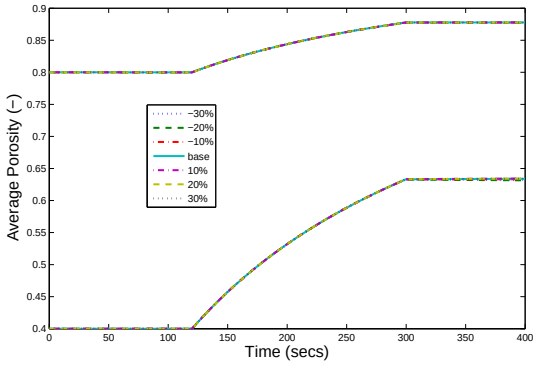

(b) Average porosity

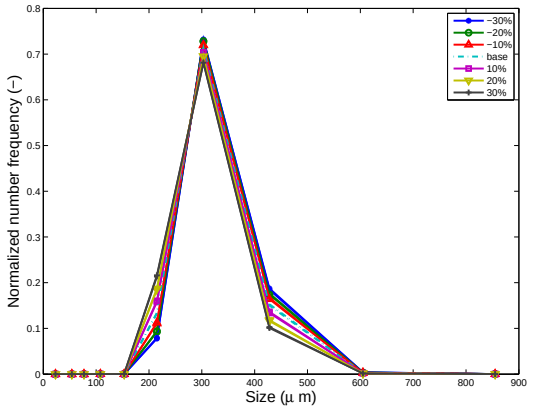

(c) PSD at the end of liquid addition

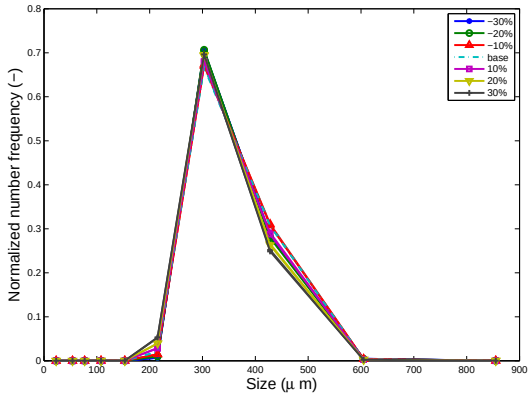

(d) PSD at the end of the wet massing time

Figure 20: Variation of contact angle between the binder liquid and the particle surface for the induction behavior showing the effect on the bulk and distributed properties

6.3 Comparative study for sensitivity analysis

From the previous sections it is evident that viscosity, contact angle, impeller speed and liquid content are the crucial parameters that have a prominent affect on the final granule properties. In this section, we have presented a more systematic and comparative study which shows the relative affect of each fundamental quantity on the population. The Fig 21 shows the 1-D plot for the bulk quantities at the end time for the steady and the induction case. It can be seen that in case of both the steady state and the induction case, the affect

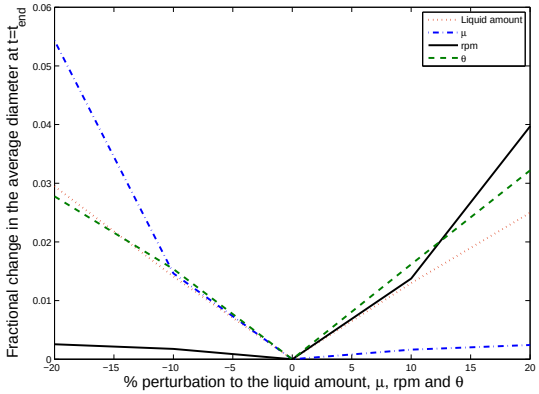

(a) Average diameter for steady growth

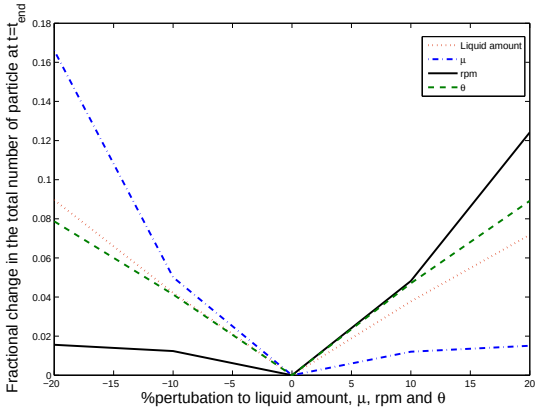

(b) Total number of particles for steady growth

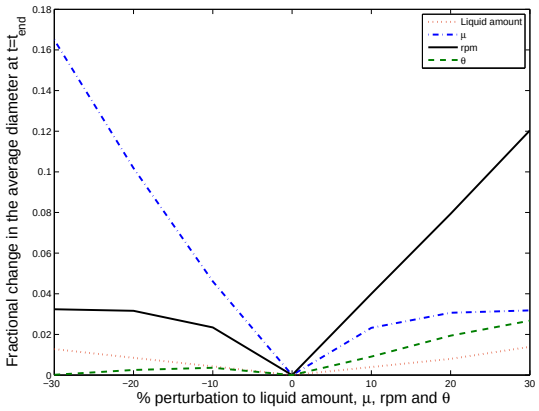

(c) Average diameter for induction growth

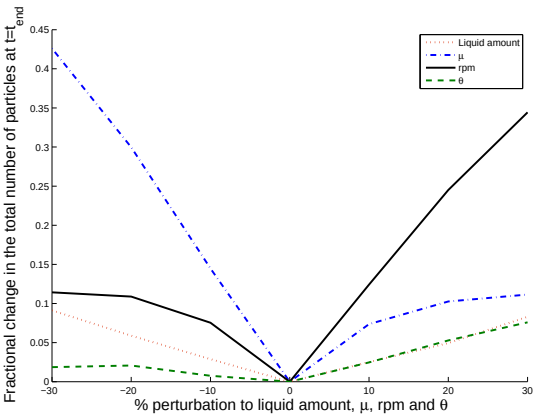

(d) Total number of particles for induction growth

Figure 21: Variation of the crucial operating parameters on the bulk particle size and number of particles at final time

of liquid is almost linear and more straightforward for the positive and negative perturbed cases. With varying liquid, the average diameter varies linearly due to the increase in the particle volume and also the total number of particles vary linearly due to the increased aggregation rate which is proportional to the amount of liquid added. The viscosity of the binder liquid has a more pronounced affect in the negatively perturbed cases than the positive perturbation cases. It can be inferred that the effect of viscosity is more nonlinear, where increasing the viscosity to a certain value helps, but beyond that point there is not

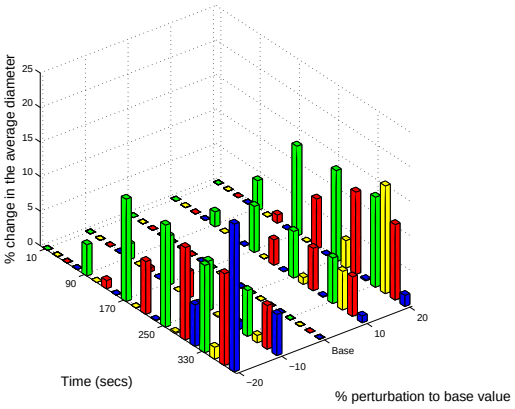

(a) Average diameter

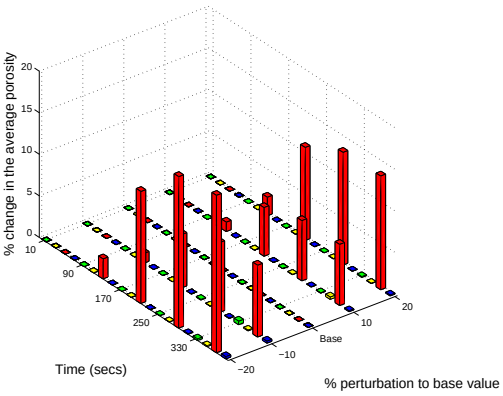

(b) Average porosity

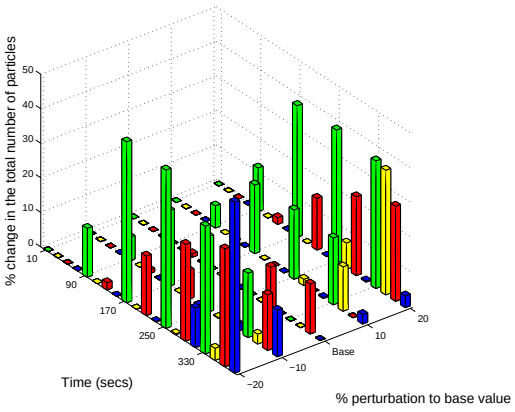

(c) Total number of particles

Figure 22: Bar plots for steady growth showing effect of crucial parameters on bulk properties (Liquid amount=red, $\mu = blue$, rpm=yellow, $\theta = green$)

much effect on the particle size when the viscosity if further increased. Also, the viscosity of the binder affects the aggregation and breakage of the particles. Therefore, it can also be observed that beyond a certain value of the viscosity, the change in the total number of particles is also reduced suggesting reduced difference in the aggregation and breakage of particles. The impeller speed has a converse effect on the particle size and the total number of particles as the viscosity. In the positively perturbed region, there is a significant effect

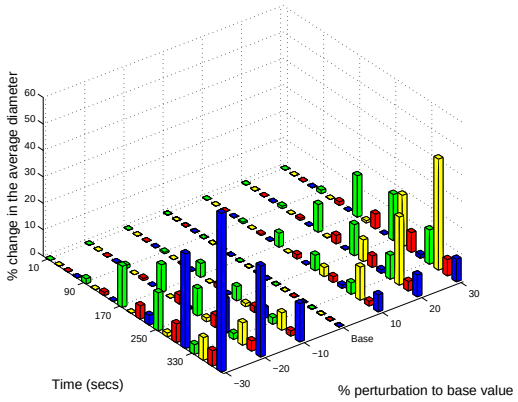

(a) Average diameter

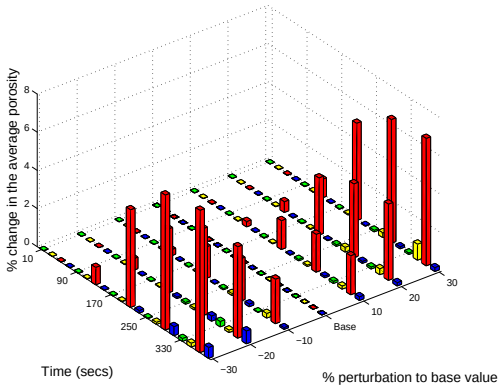

(b) Average porosity

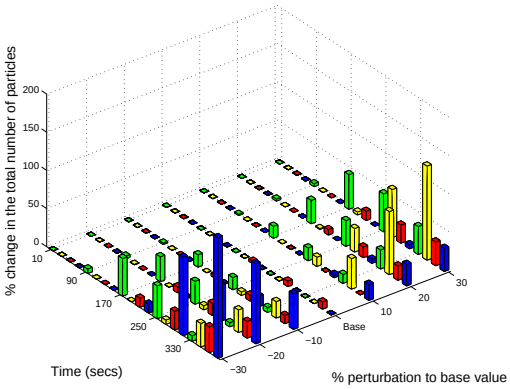

(c) Total number of particles

Figure 23: Bar plots for induction growth showing effect of crucial parameters on bulk properties (Liquid amount=red, $\mu = blue$, rpm=yellow, $\theta = green$)

as the rpm of the impeller is increased, resulting in a decrease in the particle size. The total number of particles also increase in the positively perturbed region. These observations are a result of increased breakage of particles due to higher kinetic energy and impact of the particles. The contact angle of the binder on the liquid has a pronounced effect on the aggregation of particles as it directly affects the fractional wetted surface area of the particles. In case of the steady growth process, the aggregation of particles is dominant and thus the effect of contact angle on the particle size and the total number of particles is

appreciable. For the induction growth case, the consolidation of particles is more dominant with the contact angle not having a heavy affect on the bulk properties like average diameter or total number of particles.

The bar charts as shown in Figs 22 and 23 reveal the relative affect in the form of bar charts over the entire time span. These can help with a more detailed and comparative understanding of the influence of the input fundamental parameters on the output measurable granule properties. Having a glance at the bar plots can help us have a better idea on the extent to which each input parameter affects the output granule property. The bar plots are also in agreement with the individual plots showing the bulk properties. Using this information, better control and optimization studies can be performed, since a deeper knowledge of the process can be obtained.

6.4 Experimental studies with fluid bed granulation equipment

Figure 24: Qicpic for PSD analysis

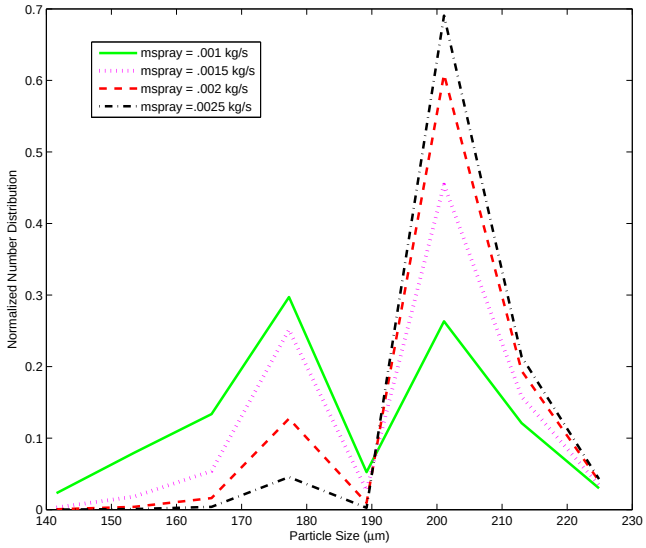

(a) PSD with varying liquid spray rate

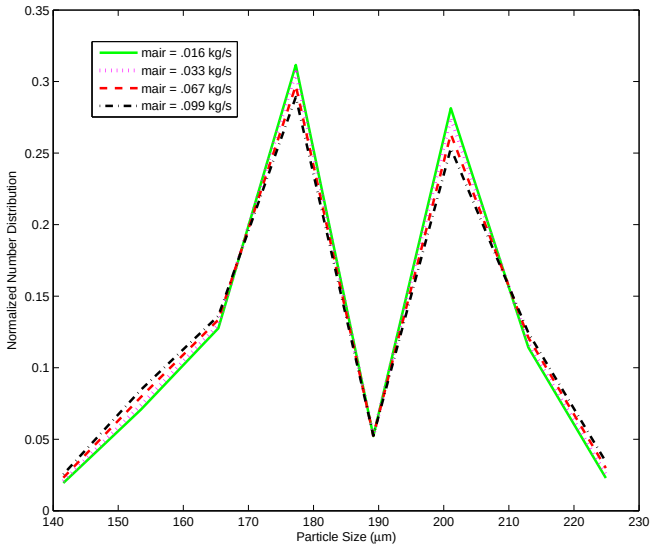

(b) PSD with varying air flowrate

Figure 25: Plots showing the effect on PSD with varying liquid spray rate and air flowrate as shown in Chaudhury et al. (2012)

Experimental studies for granulation in a fluid bed equipment was performed for a deeper insight into the mechanisms governing granulation and the influence of the operating param-

eters. The experiments were performed using the DOE mentioned in Table 3. The resultant granules were analysed using *Qicpic* from Sympatec.

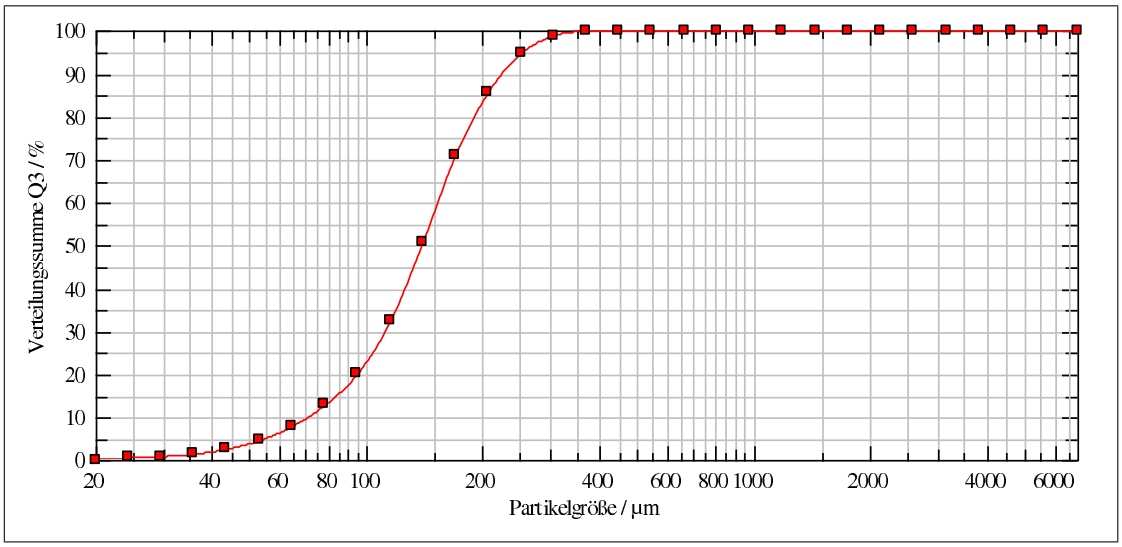

Figure 26: Cumulative PSD for the initial sample

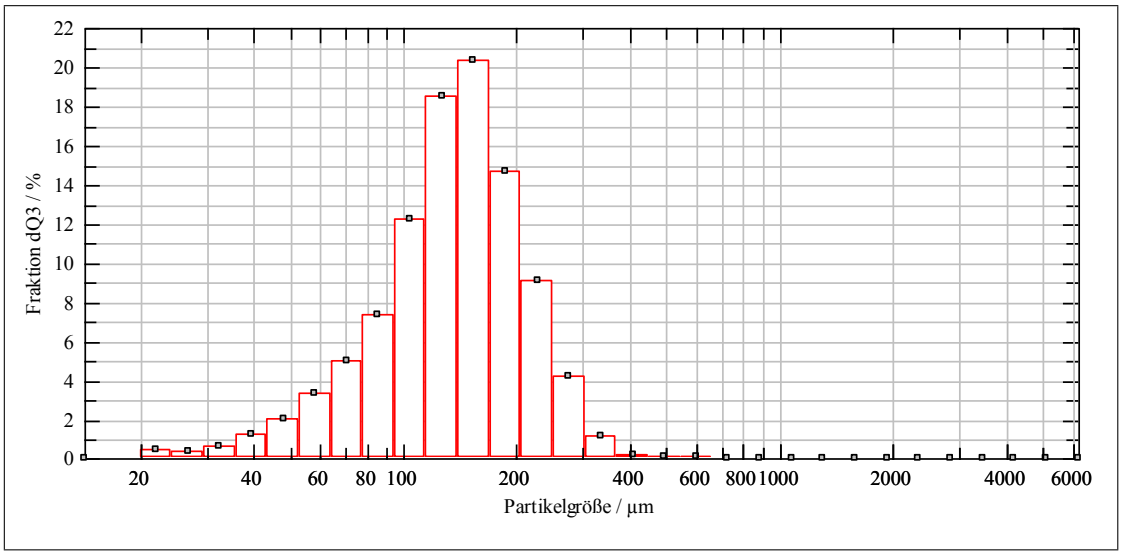

Figure 27: PSD for the initial sample

Qicpic is capable of measuring the PSD for fine particles. The granules formed from the base case and a few other scenarios were too big compared to the capacity of the measuring device. The alternative could be sieving the particles in order to obtain the PSD. The disadvantages of sieving the bigger granules would be the lack of compatibility between the sets of PSDs.

Sieving would lead to a narrow distribution due to the lack in resolution and the results would be misguiding. This inhibits the ability to compare the results for the various scenarios and obtain deductions from the results. Due to the shortage of time and lack of availability of the equipment, the DOE could not be re-formulated and the experiments could not be re-run for the purpose of better analysis. Figures 26, 28, 30, 32 show the PSD for the initial fine powder, the high variations for air flowrate and product temperature and the low variation for the liquid spray rate respectively.

From our previous works on the modeling aspects for a fluid bed granulation (Figure 25), it was observed that with a reduction in the liquid flowrate, the PSD reveals greater number of smaller particles. Thus, the PSD is shifted towards the left. Due to reduced liquid addition, the availability of surface liquid is less thus reducing the extent of aggregation. Similarly, with increasing air flowrate, the draft for drying of liquid increases. This leads to a slight reduction in the average diameter of the particles. The PSD exhibits the existence of larger number of smaller particles when the air flowrate is increased.

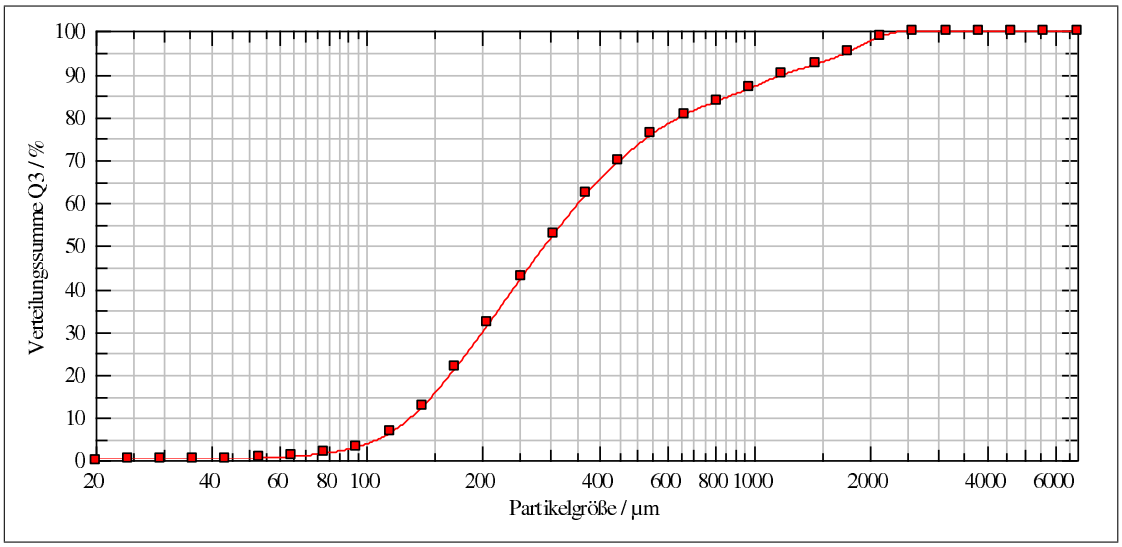

Figure 28: Cumulative PSD at final time for the high variation of air flowrate

The study was inconclusive owing to the lack of PSD information for the entire DOE set.

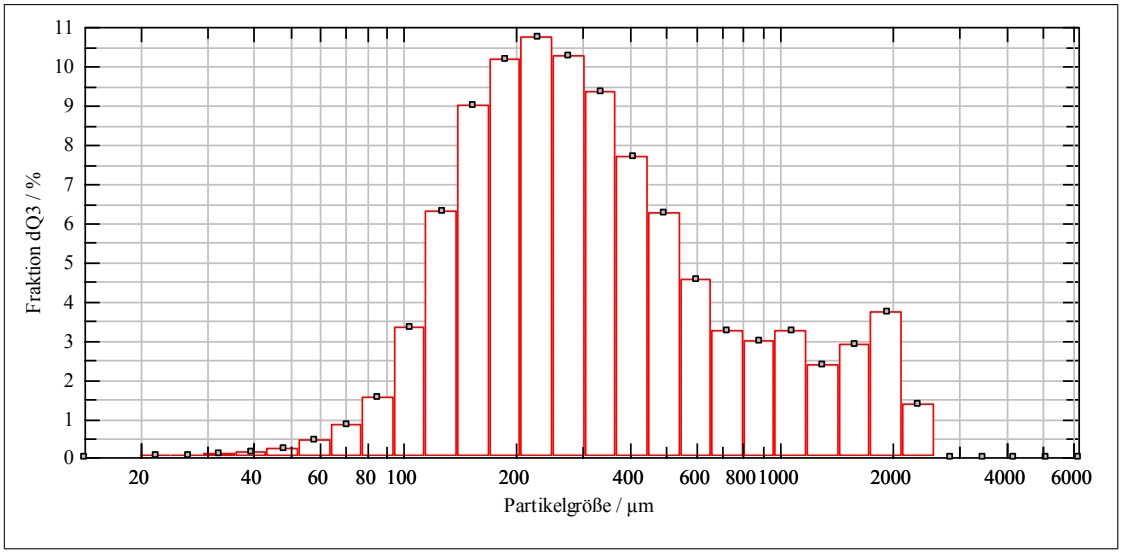

Figure 29: PSD at final time for high variation of air flowrate

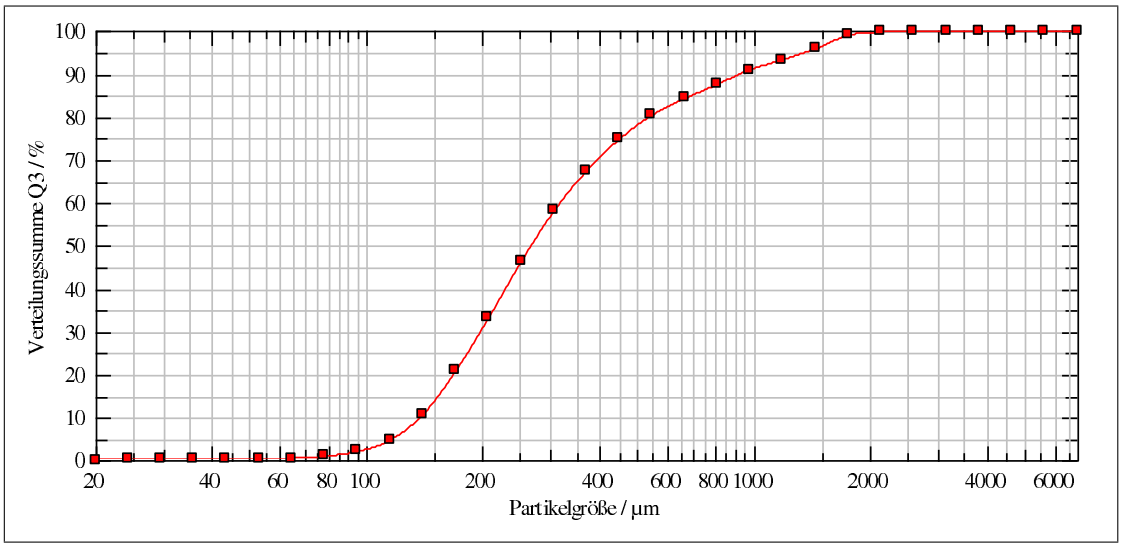

Figure 30: Cumulative PSD at final time for the high variation of product temperature

From Figures 26-32 it can clearly be seen that there is an overall increase in the particle size as granulation proceeds. The PSD for the initial sample reveals the existence of very fine powder, but the PSDs for the granulated material has a higher amount of larger particles. A mechanistic model for the fluid bed granulation was developed in our previous works (Chaudhury et al., 2012) showing the effect of the various parameters of the final granule size distribution. This study was aimed at validating the observation previously proposed using the modeling framework. The granules obtained using the other scenarios were too

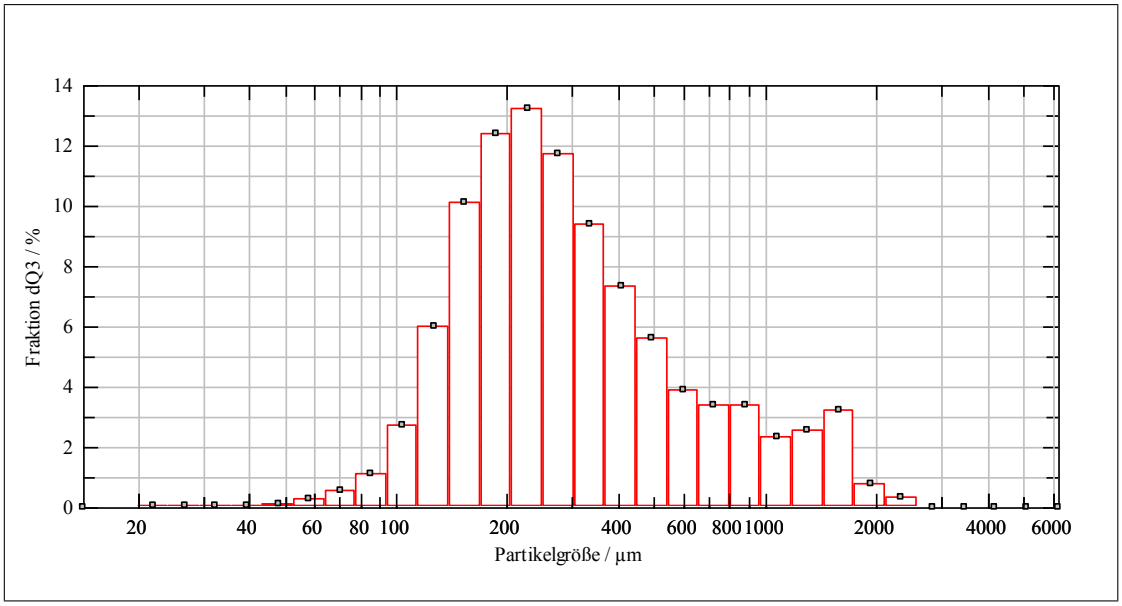

Figure 31: PSD at final time for high variation of product temperature

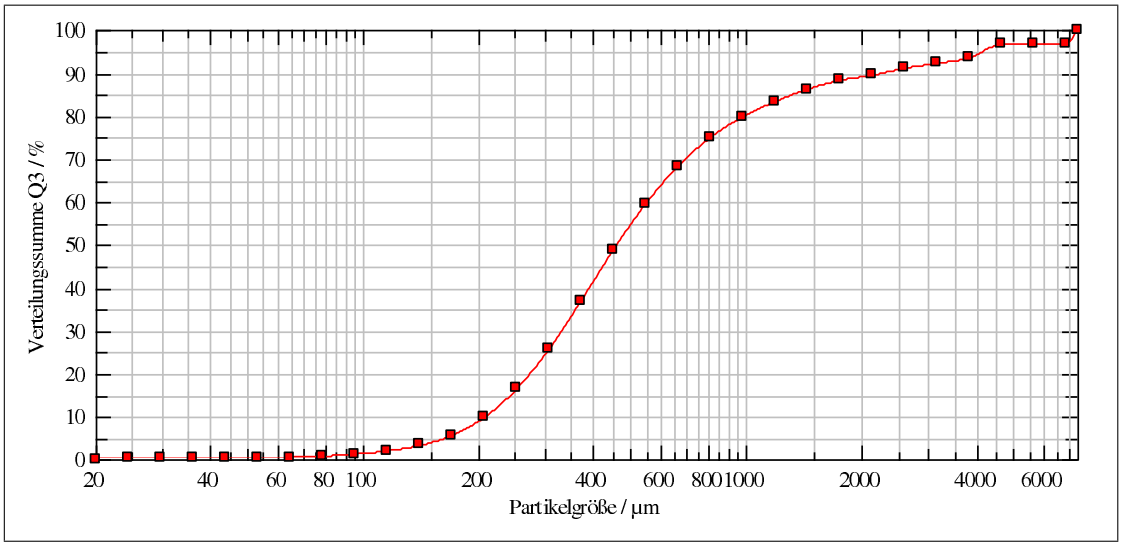

Figure 32: Cumulative PSD at final time for the low variation of liquid spray rate

big to analyse using Qicpic, thus suggesting the formation of bigger granules. Lower spray rate controls the liquid distribution and prevents "lump" formation. Higher air flowrate enhances the fluidization in the bed, thus dispersing the powder within the bed. Along with the high product temperature, the high air flowrate also increases the drying of the powders within the bed. This leads to a reduction in the surface liquid availability of the powder and hence large agglomerates are significantly cut down. The resultant granule population

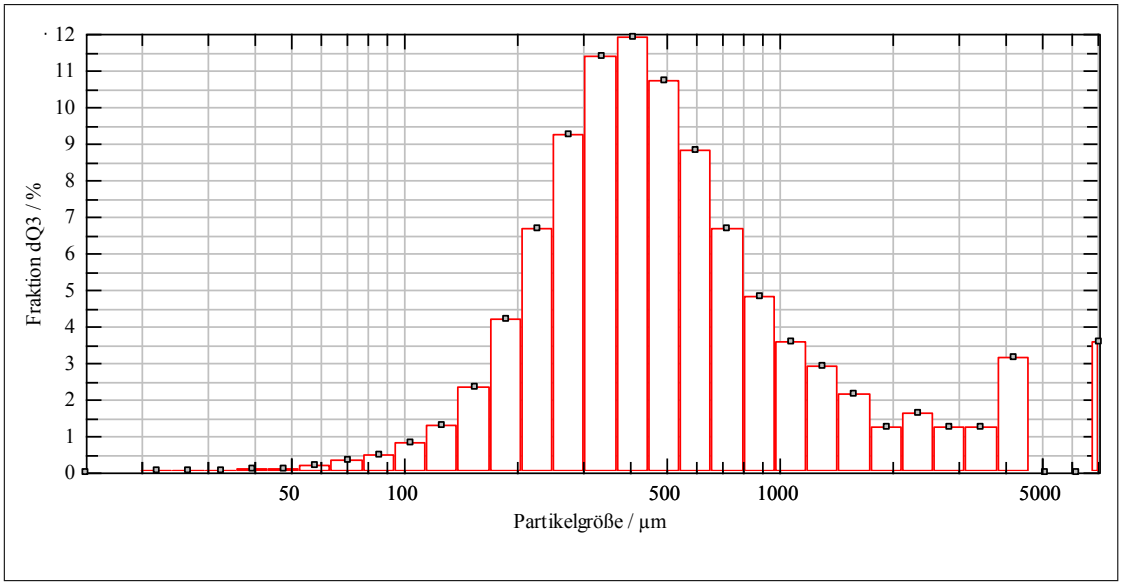

Figure 33: PSD at final time for low variation of liquid spray rate

is more homogeneous with respect to size and the distribution is narrower compared to the other unmeasurable scenarios. The air flowrate and the product temperature for the base case is speculated to be too less for more homogeneous granules to be formed. Thus, for a constant spray rate of liquid, smaller, measurable granules could not be obtained for lower L/S ratio.

6.5 Parameter estimation results

The parameter estimation results can provide good insight towards the techniques and methods that can be employed for improved estimation of empirical parameters. A detailed review on the techniques has been conducted taking into consideration metaheuristic techniques and the standard gEST platform offered by gPROMS. For now, only estimates have been obtained only for the model describing the growth case. The optimization algorithms have been run using the square of error between the target and the simulated concentration evolution profile. The optimization procedure used by the metaheuristic techniques give a global op-

tima although the computational time required is large. The gEST optimization platform provides a local optima for the minimization problem. Figure 34 shows the control on the supersaturation profile and the CSD of the seed and the final product crystals.

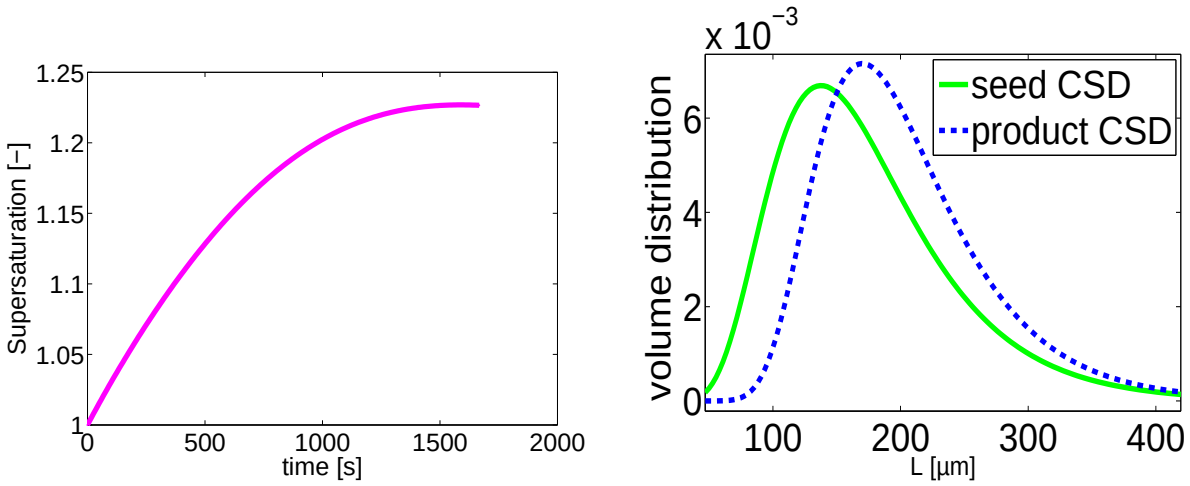

(a) Supersaturation profile

(b) Initial and final crystal size distribution

Figure 34: Supersaturation profile and the crystal size distribution of the initial and final crystals simulated using the PBM

Figure 35 shows the trend in the objective function over the entire domain spanning the lower and upper bounds for the various empirical parameters. It can be seen that there is an extensive shallow region in the figure but the minima seems unique.

The optimization algorithms have been implemented on the objective function simulating the error, and the respective estimates have been obtained for the empirical parameters. We have subdivided this review into two categories, one applicable for smooth data and the other for noisy data. It is more realistic to analyse the behavior of the optimization algorithms towards estimating empirical parameters for noisy data, owing to the fact that real data has a lot of noise in it for various factors. For the simulated annealing algorithm,

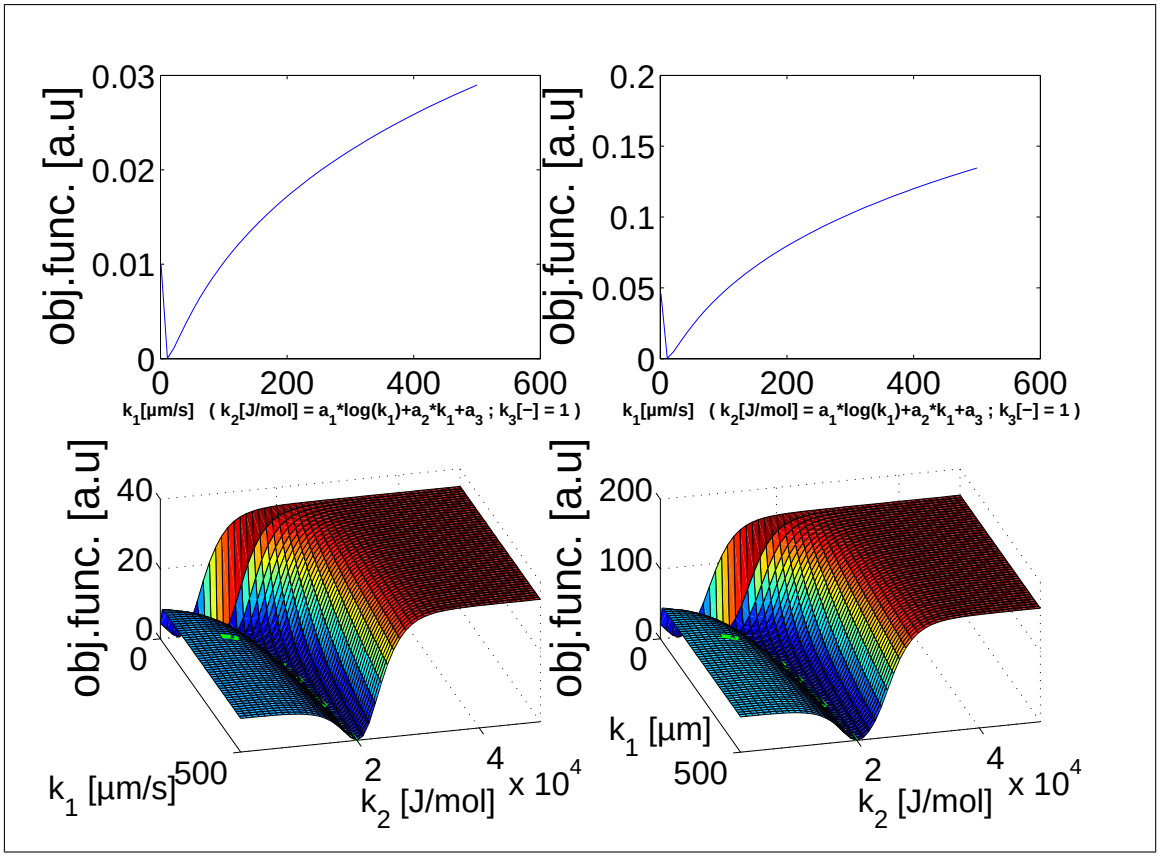

Figure 35: Objective function plotted over the entire domain for k_1, k_2 and k_3 fixed at 1 for experiment 5 (left) and experiments 1-4 (right)

the various parameters used in the optimization algorithm have been mentioned in Section 3.2.1. The particle swarm algorithm was implemented using $c_1 = 2$, $c_2 = 2$ and $w = 0.4$. It should be kept in mind that owing to the stochastic nature of the Simulated annealing and the Particle swarm algorithm, the results obtained from the coarse optimization step tend to vary (although minutely) after each runs. The bounds were strictly imposed while doing the optimization using either of the algorithms. For the gEST toolbox, we have used a constant relative variance model ranging between $0.1 - 0.15$. The parameter estimation was performed with multiple experiments using different combinations from the list provided in Table 2. In order to have better results, we foresee the global optimization algorithms having the role of a coarse optimizer followed by a gradient based method in the end of the

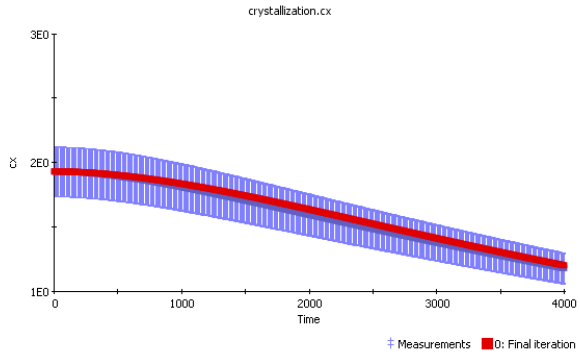

(a) Concentration profile for experiment 1

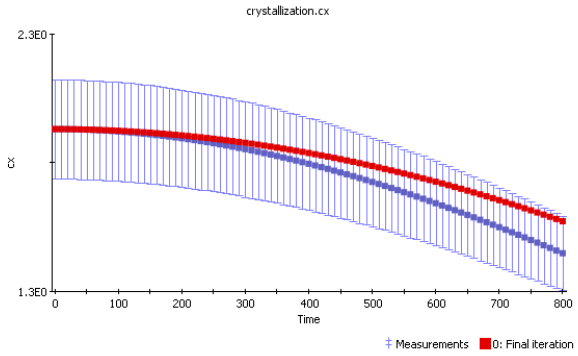

(b) Concentration profile for experiment 2

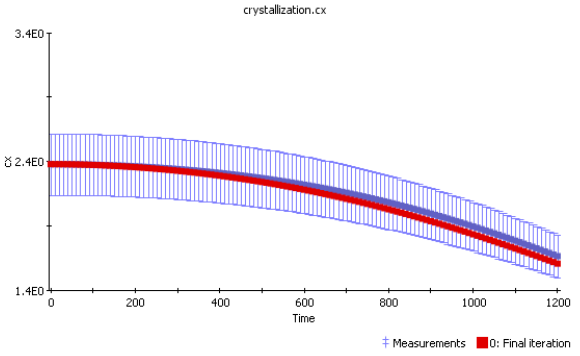

(c) Concentration profile for experiment 3

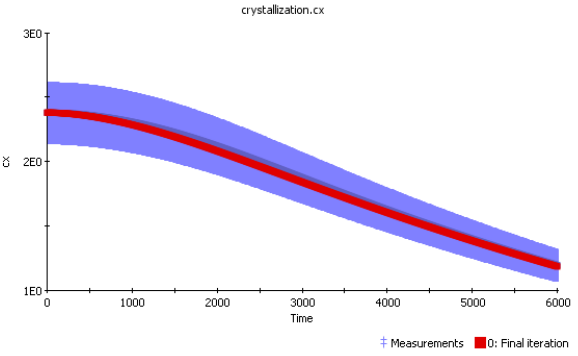

(d) Concentration profile for experiment 4

Figure 36: Concentration profiles for the experiments listed in table 4 after the parameter estimation using experiments $1 + 2 + 3 + 4$ in gPROMS

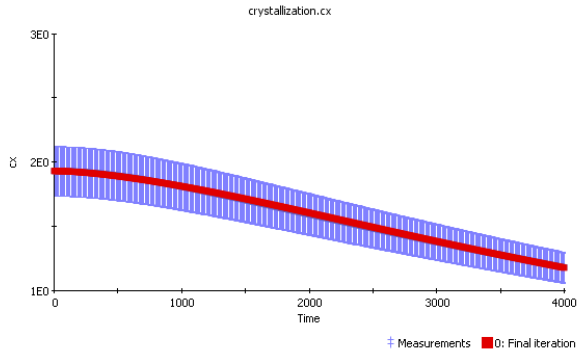

(a) Concentration profile for experiment 1

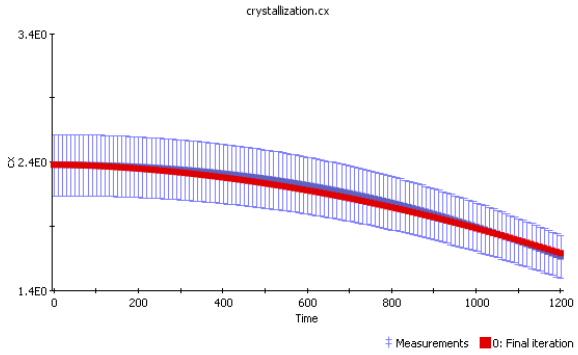

(b) Concentration profile for experiment 3

Figure 37: Concentration profiles for the experiments listed in table 4 after the parameter estimation using experiments $1 + 3$ in gPROMS

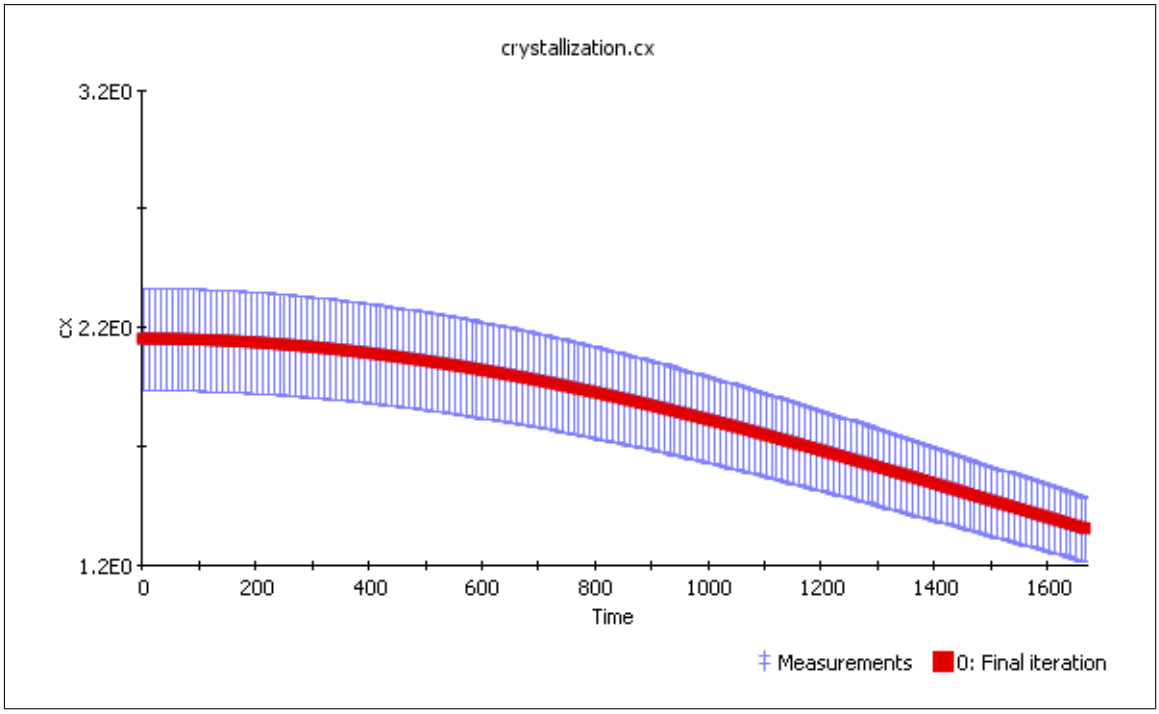

Figure 38: Concentration profiles for the experiments listed in table 4 after the parameter estimation using experiment 5 in gPROMS

SAA and PSO algorithm (using the optimal values obtained from these algorithms as the initial guess) for the fine tuning. Sequential quadratic programming (SQP) was used for the gradient based method. The inbuilt SQP algorithm available in MATLAB Version 2012a was used for the local optimization. This methodology leads us to the value for the estimates as listed in Table 6 and 7

From the tables it can be seen that SAA gives better results without the gradient based method used for the fine tuning. It should be kept in mind that SAA requires an initial guess for its calculation unlike the PSO. The better results from the coarse optimization algorithm could be an artifact of the initial guess. Since this work is still in continuation, further investigations are being made and soon a statement can be provided in this regard. The particle swarm algorithm is faster than SAA (computation wise). The birds in the PSO start flying randomly but eventually their flight is biased by the communication between

	SA		PS		GPROMS	
	parameters	Error	parameters	Error	parameters	Error
Experiment 5	$k_1 = 6.4$ $k_2 = 1.4206 \cdot e^4$ $k_3 = 1$	$7.9014e^{-4}$	$k_1 = 22.914$ $k_2 = 8.8348 \cdot e^3$ $k_3 = 3.6$	0.7056	$k_1 = 16.8921$ $k_2 = 1.1834 \cdot e^4$ $k_3 = 0.993021$	-246.862
Experiment 1+3	$k_1 = 11.0021$ $k_2 = 1.0244 \cdot e^4$ $k_3 = 1$	$4.2778e^{-4}$	$k_1 = 28.9$ $k_2 = 1.8383 \cdot e^4$ $k_3 = 1$	1.2988	$k_1 = 5.4903$ $k_2 = 1.0231 \cdot e^4$ $k_3 = 0.69882$	-806.83
Experiment 1+2+3+4	$k_1 = 12$ $k_2 = 1.0421 \cdot e^4$ $k_3 = 1$	0.0033	$k_1 = 43$ $k_2 = 1.7491 \cdot e^4$ $k_3 = 2$	0.4137	$k_1 = 9.13179$ $k_2 = 1.0422 \cdot e^4$ $k_3 = 0.946616$	-1732.82

Table 6: Estimated parameters using SA, PSO and gEST

	SA with SQP		PS with SQP	
	parameters	Error	parameters	Error
Experiment 5	$k_1 = 10$ $k_2 = 9.9992 \cdot e^3$ $k_3 = 1$	$1.5812e^{-10}$	$k_1 = 10$ $k_2 = 9.992 \cdot e^3$ $k_3 = 1$	$1.78e^{-10}$
Experiment 1+3	$k_1 = 11.0286$ $k_2 = 1.0244 \cdot e^4$ $k_3 = 1$	$1.5259e^{-5}$	$k_1 = 10$ $k_2 = 9.9994 \cdot e^3$ $k_3 = 1$	$1.533e^{-10}$
Experiment 1+2+3+4	$k_1 = 10$ $k_2 = 9.9993 \cdot e^3$ $k_3 = 1$	$1.772e^{-10}$	$k_1 = 10$ $k_2 = 9.9993 \cdot e^3$ $k_3 = 1$	$1.809e^{-10}$

Table 7: Estimated parameters using SA, PSO and gEST

each individual point in the flock. The birds seem to start concentrating near the point where a global optimum is seen by any bird that is a part of the flock. This interaction between the different points is missing in case of SAA. Thus, the convergence is faster in case of PSO due to the interactive behavior of the data points while optimizing the objective function. There is still some room for improvement with the algorithms by changing the values for the adjustable parameters such as c_1, c_2 and w in PSO and the cooling rate in the SA algorithm. With the gradient based, fine tuning algorithm at the end, the performance

of both the PSO and SAA methods seems impeccable in estimating the ideal values used to formulate the inverse problem. The estimation using gEST comes with an elaborate statistical analysis in the execution output report, which provides details on the confidence ellipsoids, variance-covariance matrix, variance value used and more similar data relevant to the estimates to provide an idea on the quality of the estimated parameters.

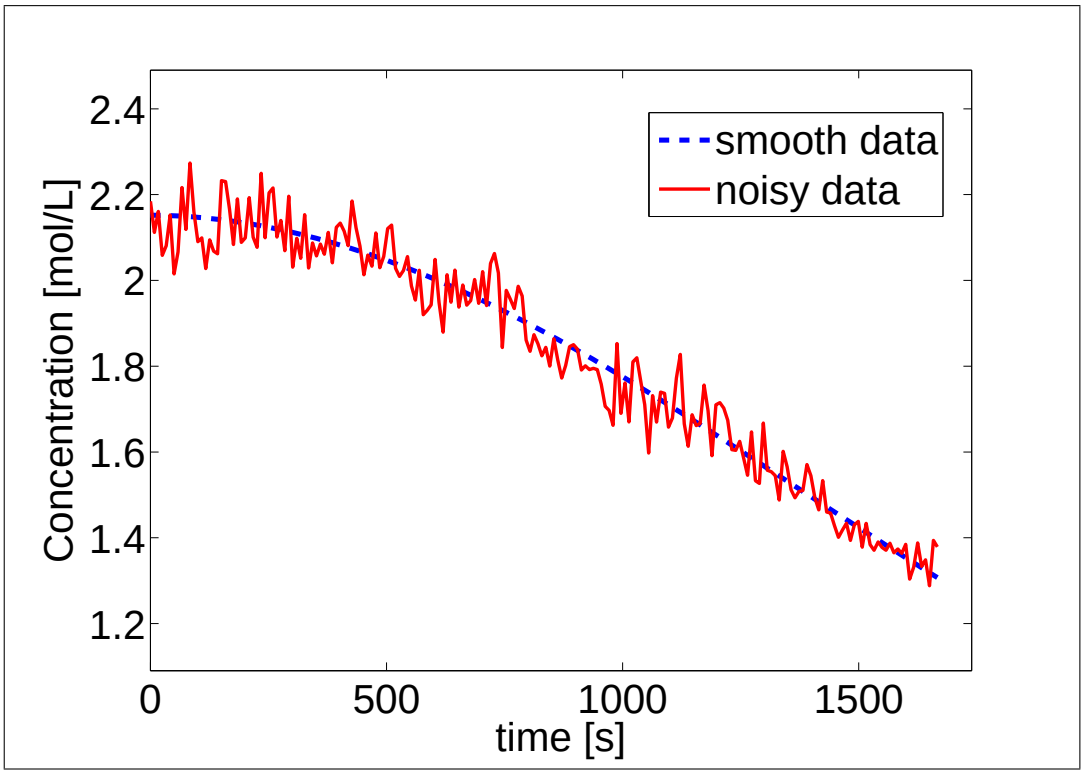

Figure 41: Concentration profile with noise added

As the smoothed, simulated data was used for the parameter estimation exercise, a study has also been performed to test the performance of these algorithms on noisy data which is a better replication of real data obtained from measurements. The noisy data was generated using the previous smooth, simulated data and can be represented using the expression (74)

$$C_{i,noise} = C_i \pm \frac{C_i}{100}\sigma \; rand_n \tag{74}$$

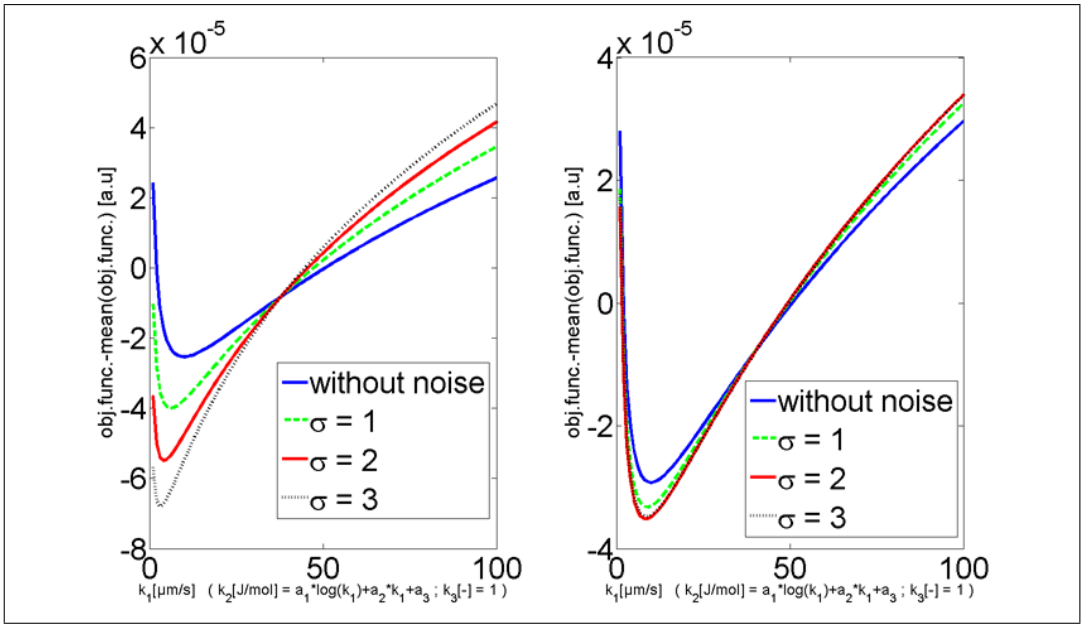

Figure 42: Objective function with noisy data over entire domain of k_1, k_2 and $k_3 = 1$

The noisy data using Equation (74) and a σ value of 3 has been shown in Figure 41. Similar to the smoothed data, the objective function has also been plotted for the noisy data in the entire domain for k_1 and k_2, keeping k_3 fixed at 1. It can be seen from the previous discussions that the gradient based method at the end of the meta heuristic method, significantly improves the estimates for the inverse problem. Thus, for the noisy data, we are solely focussing on the performance of the optimization algorithm after the gradient based method has been implemented. Table 8 summarizes the results obtained from the minimization of the error using noisy data.

It can be noted that the performance of the PSO greatly deteriorates while handling noisy data. The estimates obtained from the SA+SQP algorithm reveal a closer approximation to the original values used for framing the inverse problem.

	SA with SQP		PS with SQP	
	parameters	Error	parameters	Error
Experiment 5	$k_1 = 12.6065$ $k_2 = 1.0532 \cdot e^4$ $k_3 = 1.0132$	$1.1879e^{-5}$	$k_1 = 12.5746$ $k_2 = 1.0811 \cdot e^4$ $k_3 = 0.9510$	0.0013
Experiment 1+3	$k_1 = 9.9968$ $k_2 = 9.9992 \cdot e^3$ $k_3 = 1$	$1.6897e^{-10}$	$k_1 = 28.2067$ $k_2 = 1.2653 \cdot e^4$ $k_3 = 1.0041$	0.5667
Experiment 1+2+3+4	$k_1 = 9.9981$ $k_2 = 9.9995 \cdot e^3$ $k_3 = 1$	$1.4166e^{-10}$	$k_1 = 26.9$ $k_2 = 1.8389 \cdot e^4$ $k_3 = 1.0222$	0.0014

Table 8: Estimated parameters using SA+SQP and PSO+SQP for noisy data

7 Conclusion

This report deals with obtaining a semi-mechanistic aggregation kernel that is representative of the influence of the input parameters on the output quantities. The model can effectively capture the steady and induction growth behaviors under the conditions observed in experiments. The dynamic sensitive analysis included in this work also gives a comparative study on the extent at which each of the crucial fundamental parameter effects the final granule character. This also provides with an insight on which input parameter could be manipulated in order to obtain a granule population with a certain characteristic. This model could also be beneficial for being extended for control, optimization or scheduling kind of work. The ability of the model to be able to capture the intricate behavioral attributes observed during the practical granulation process makes this work novel and this model different from the pre-existing models noticed in literature.

The results from the experimental studies were inconclusive due to the absence of enough measurable PSDs for the various scenarios listed in the DOE. Intuitively, the trends show agreement with the outcomes predicted in previous works (Chaudhury et al., 2012). The review for the various parameter estimation techniques suggest the applicability of the various algorithms for effective estimation of empirical parameters using noisy and smoothed data. The performance of the SAA and PSO were comparable for smooth data, but with noisy data, the performance of PSO deteriorated significantly. Appropriate choice of the objective function and number of experiments to be included for the estimation need further attention.

8 Future work

The parameter estimation work is being extended further and a joint paper with the colleagues at RCPE is aimed at. This work requires further attention in terms of exploring the different types of objective functions that could be used for the error minimization and the number of experiments that need to be considered for improved estimates. Furthermore, the results from the various algorithms need to be explored further in order to be able to make solid statements that might ease the parameter estimation exercise for researchers. The 1-D crystallization PBM considered includes only the growth mechanism. Estimation using more mechanisms such as aggregation and nucleation and considering more measurable quantities into the objective function (such as CSD) is yet another direction we are aiming at looking into.

References

Adetayo, A. A., Ennis, B. J., 1997. Unifying approach to modeling granule coalescence mechanisms. AIChE Journal 43 (4), 927–934.

Biggs, C., Sanders, C., Scott, A., Willemse, A., Hoffman, A., Instone, T., Salman, A., Hounslow, M., 2003. Coupling granule properties and granulation rates in high-shear granulation. Powder Technology 130 (1-3), 162 – 168.

Boerefijn, R., Hounslow, M., 2005. Studies of fluid bed granulation in an industrial r&d context. Chemical Engineering Science 60 (14), 3879 – 3890.

Boukouvala, F., Dubey, A., Vanarase, A., Ramachandran, R., Muzzio, F. J., Ierapetritou, M., 2011a. Computational approaches for studying granular dynamics of continuous blending processes, 2- population balance and data-based methods. Macromolecular Materials and Engineering 297, 9–19.

Boukouvala, F., Ramachandran, R., Muzzio, F. J., Ierapetritou, M., 2011b. Computer-aided design of an integrated pharmaceutical process. Computer aided Chemical Engineering 6, 100–105.

Braumann, A., Kraft, M., Wagner, W., 2010. Numerical study of a stochastic particle algorithm solving a multidimensional population balance model for high shear granulation. Journal of Computational Physics 229, 7672–7691.

Chakraborty, J., Kumar, S., 2007. A new framework for solution of multidimensional population balance equations. Chemical Engineering Science 62 (15), 4112 – 4125.

Chaudhury, A., Niziolek, A., Ramachandran, R., 2012. Multi-dimensional mechanistic modeling of fluid bed granulation processes: An integrated approach. Advanced Powder Technology, 10.1016/j.apt.2012.03.005.

Costa, C. B. B., Maciel, M. R. W., Filho, R. M., 2007. Considerations on the crystallization modeling: Population balance solution. Computers & Chemical Engineering 31 (3), 206 – 218.

Ennis, B. J., Tardos, G., Pfeffer, R., 1991. A microlevel-based characterization of granulation phenomena. Powder Technology 65 (1-3), 257 – 272.

Gunawan, R., Fusman, I., Braatz, R. D., 2004. High resolution algorithms for multidimensional population balance equations. AIChE Journal 50 (11).

Hapgood, K. P., Litster, J. D., Biggs, S. R., Howes, T., 2002. Drop penetration into porous powder beds. Journal of Colloid and Interface Science 253 (2), 353 – 366.

Hapgood, K. P., Litster, J. D., Smith, R., 2003. Nucleation regime map for liquid bound granules. AIChE Journal 49 (2), 350–361.

Hapgood, K. P., Nguyen, T. H., Hauw, S., Iveson, S. M., Shen, W., 2009. Rewetting effects and droplet motion on partially wetted powder surfaces. AIChE Journal 55 (6), 1402–1415.

Heinrich, S., Morl, L., 1999. Fluidized bed spray granulationa new model for the description of particle wetting and of temperature and concentration distribution. Chemical Engineering and Processing: Process Intensification 38 (4-6), 635 – 663.

Hounslow, M. J., Pearson, J. M. K., Instone, T., 2001. Tracer studies of high-shear granulation: Ii. population balance modeling. AIChE Journal 47 (9), 1984–1999.

Hu, Q., Rohani, S., Wang, D. X., Jutan, A., 2004. Nonlinear kinetic parameter estimation for batch cooling seeded crystallization. AIChE Journal 50 (8), 1786–1794.

Hulburt, H., Katz, S., 1964. Some problems in particle technology: A statistical mechanical formulation. Chemical Engineering Science 19 (8), 555 – 574.

Immanuel, C. D., Doyle III, F. J., 2003. Computationally efficient solution of population balance models incorporating nucleation, growth and coagulation: application to emulsion polymerization. Chemical Engineering Science 58 (16), 3681 – 3698.

Immanuel, C. D., Doyle III, F. J., 2005. Solution technique for a multi-dimensional population balance model describing granulation processes. Powder Technology 156 (2-3), 213 – 225.

Iveson, S. M., 2002. Limitations of one-dimensional population balance models of wet granulation processes. Powder Technology 124, 219–229.

Iveson, S. M., Litster, J. D., Hapgood, K., Ennis, B. J., 2001. Nucleation, growth and breakage phenomena in agitated wet granulation processes: a review. Powder Technology 117 (1-2), 3 – 39.

Kalbasenka, A., Huesman, A., Kramer, H., 2011. Modeling batch crystallization processes: Assumption verification and improvement of the parameter estimation quality through empirical experiment design. Chemical Engineering Science 66 (20), 4867 – 4877.

Kapur, P. C., Fuerstenau, D. W., 1969. Coalescence model for granulation. Industrial and Engineering Chemistry Process Design and Development 8 (1), 56–62.

Kennedy, J., Eberhart, R., nov/dec 1995. Particle swarm optimization. In: Neural Networks, 1995. Proceedings., IEEE International Conference on. Vol. 4. pp. 1942 –1948.

Kirkpatrick, S., Gelatt, C. D., Vecchi, M. P., 1983. Optimization by simulated annealing. Science 220, 671–680.

Knight, P., Instone, T., Pearson, J. M., Hounslow, M., 1993. An investigation into the kinetics of granulation using a high shear mixer. Powder Technology 77, 159–169.

Kumar, J., Peglow, M., Warnecke, G., Heinrich, S., 2008. An efficient numerical technique for solving population balance equation involving aggregation, breakage, growth and nucleation. Powder Technology 182 (1), 81 – 104.

Kumar, J., Peglow, M., Warnecke, G., Heinrich, S., Mrl, L., 2006. Improved accuracy and convergence of discretized population balance for aggregation: The cell average technique. Chemical Engineering Science 61 (10), 3327 – 3342.

Kumar, S., Ramkrishna, D., 1996a. On the solution of population balance equations by discretization–i. a fixed pivot technique. Chemical Engineering Science 51 (8), 1311 – 1332.

Kumar, S., Ramkrishna, D., 1996b. On the solution of population balance equations by discretizationii. a moving pivot technique. Chemical Engineering Science 51 (8), 1333 – 1342.

LeVeque, R., 2002. Finite volume methods for hyperbolic problems. Cambridge University Press.

Li, J., Freireich, B., Wassgren, C., Litster, J. D., 2012. A general compartment-based population balance model for particle coating and layered granulation. AIChE Journal 58 (5), 1397–1408.

Link, K. C., Schlunder, E. U., 1997. Fluidized bed spray granulation. investigation of the coating process on a single sphere. Chemical Engineering and Processing 36, 443–357.

Litster, J., 2003. Scaleup of wet granulation processes: science not art. Powder Technology 130 (1-3), 35 – 40.

Liu, L. X., Litster, J. D., Iveson, S. M., Ennis, B. J., 2000. Coalescence of deformable granules in wet granulation processes. AIChE Journal 46 (3), 529–539.

Madec, L., Falk, L., Plasari, E., 2003. Modelling of the agglomeration in suspension process with multidimensional kernels. Powder Technology 130 (1-3), 147 – 153.

Maia, G. D., Giulietti, M., 2008. Solubility of acetylsalicylic acid in ethanol, acetone, propylene glycol, and 2-propanol. Journal of Chemical & Engineering Data 53 (1), 256–258.

Majumder, A., Kariwala, V., Ansumali, S., Rajendran, A., 2012. Lattice boltzmann method for multi-dimensional population balance models in crystallization. Chemical Engineering Science 70, 121 – 134.

Mantzaris, N. V., Daoutidis, P., Srienc, F., 2001. Numerical solution of multi-variable cell population balance models. iii. finite element methods. Computers and Chemical Engineering 25 (11-12), 1463 – 1481.

Marchal, P., David, R., Klein, J., Villermaux, J., 1988. Crystallization and precipitation

engineering i. an efficient method for solving population balance in crystallization with agglomeration. Chemical Engineering Science 43 (1), 59 – 67.

Marshall Jr, C. L., Rajniak, P., Matsoukas, T., 2010. Numerical simulations of two-component granulation: Comparison of three methods. Chemical Engineering Research and Design In Press, Corrected Proof, –.

Marshall Jr., C. L., Rajniak, P., Matsoukas, T., 2011. Numerical simulations of two-component granulation: Comparison of three methods. Chemical Engineering Research and Design 89 (5), 545 – 552.

Matthews, H. B., Rawlings, J. B., 1998. Batch crystallization of a photochemical: Modeling, control, and filtration. AIChE Journal 44 (5), 1119–1127.

Mesbah, A., Kramer, H. J., Huesman, A. E., den Hof, P. M. V., 2009. A control oriented study on the numerical solution of the population balance equation for crystallization processes. Chemical Engineering Science 64 (20), 4262 – 4277.

Metropolis, N., Rosenbluth, A. W., Rosenbluth, M. N., Teller, A. H., Teller, E., 1953. Equation of State Calculations by Fast Computing Machines. The Journal of Chemical Physics 21 (6), 1087–1092.

Modares, H., Sistani, M.-B. N., 2011. Solving nonlinear optimal control problems using a hybrid ipsosqp algorithm. Engineering Applications of Artificial Intelligence 24 (3), 476 – 484.

Morl, L., Heinrich, S., Peglow, M., 2007. Chapter 2 fluidized bed spray granulation. In: A.D. Salman, M. H., Seville, J. (Eds.), Granulation. Vol. 11. pp. 21 – 188.

Nagy, Z. K., 2008. A population balance model approach for crystallization product engineering via distribution shaping control. In: 18th European Symposium on Computer Aided Process Engineering. Vol. 25 of Computer Aided Chemical Engineering. pp. 139 – 144.

Nowee, S. M., Abbas, A., Romagnoli, J. A., 2007. Optimization in seeded cooling crystallization: A parameter estimation and dynamic optimization study. Chemical Engineering and Processing: Process Intensification 46 (11), 1096 – 1106.

Nursin, B., 2010. Mathematical modelling and optimisation of the formulation and manufacture of aggregate food products. Ph.D. thesis, National University of Ireland, Cork, Ireland.

Osborne, J. D., Sochon, R. P., Cartwright, J. J., Doughty, D. G., Hounslow, M. J., Salman, A. D., 2011. Binder addition methods and binder distribution in high shear and fluidised bed granulation. Chemical Engineering Research and Design 89 (5), 553 – 559.

Oullion, M., Puel, F., Fevotte, G., Righini, S., Carvin, P., 2007. Industrial batch crystallization of a plate-like organic product. in situ monitoring and 2d-csd modelling. part 2: Kinetic modelling and identification. Chemical Engineering Science 62 (3), 833 – 845.

Pandya, J., Spielman, L., 1983. Floc breakage in agitated suspensions: Effect of agitation rate. Chemical Engineering Science 38 (12), 1983 – 1992.

Pinto, M. A., Immanuel, C. D., Doyle III, F. J., 2007. A feasible solution technique for higher-dimensional population balance models. Computers and Chemical Engineering 31 (10), 1242 – 1256.

Poon, J. M. H., Ramachandran, R., Sanders, C. F. W., Glaser, T., Immanuel, C. D., Doyle III, F. J., Litster, J. D., Stepanek, F., Wang, F. Y., Cameron, I. T., 2009. Experimental validation studies on a multi-scale and multi-dimensional population balance model of batch granulation. Chemical Engineering Science 64, 775–786.

Qamar, S., Warnecke, G., 2007. Numerical solution of population balance equations for nucleation, growth and aggregation processes. Computers and Chemical Engineering 31 (12), 1576 – 1589.

Qiu, Y., Rasmuson, A. C., 1991. Nucleation and growth of succinic acid in a batch cooling crystallizer. AIChE Journal 37 (9), 1293–1304.

Rahmanian, N., Naji, A., Ghadiri, M., 2011. Effects of process parameters on granules properties produced in a high shear granulator. Chemical Engineering Research and Design 89 (5), 512 – 518.

Rajniak, P., Mancinelli, C., Chern, R., Stepanek, F., Farber, L., Hill, B., 2007. Experimental study of wet granulation in fluidized bed: Impact of the binder properties on the granule morphology. International Journal of Pharmaceutics 334 (1-2), 92 – 102.

Ramachandran, R., Ansari, M. A., Chaudhury, A., Kapadia, A., Prakash, A. V., Stepanek, F., 2012. A quantitative assessment of the influence of primary particle size polydispersity on granule inhomogeneity. Chemical Engineering Science 71, 104 – 110.

Ramachandran, R., Barton, P. I., 2010. Effective parameter estimation within a multi-dimensional population balance model framework. Chemical Engineering Science 65 (16), 4884 – 4893.

Ramachandran, R., Immanuel, C. D., Stepanek, F., Litster, J. D., Doyle III, F. J., 2009. A mechanistic model for breakage in population balances of granulation: Theoretical kernel development and experimental validation. Chemical Engineering Research and Design 87 (4), 598 – 614.

Ramachandran, R., Poon, J. M. H., Sanders, C. F. W., Glaser, T., Immanuel, C. D., Doyle III, F. J., Litster, J. D., Stepanek, F., Wang, F. Y., Cameron, I. T., 2008a. Experimental studies on distributions on granule size, binder content and porosity in batch drum granulation: inferences on process modelling requirements and process sensitivities. Powder Technology 188, 89–101.

Ramachandran, R., Poon, J. M. H., Sanders, C. F. W., Glaser, T., Immanuel, C. D., Doyle III, F. J., Litster, J. D., Stepanek, F., Wang, F. Y., Cameron, I. T., 2008b. Experimental studies on distributions on granule size, binder content and porosity in batch drum granulation: inferences on process modelling requirements and process sensitivities. Powder Technology 188, 89–101.

Rambali, B., Baert, L., Massart, D. L., 2003. Scaling up of the fluidized bed granulation process. International Journal of Pharmaceutics 252, 197–206.

Reche-Lopez, P., Ruiz-Reyes, N., Galan, S. G., Jurado, F., 2009. Comparison of metaheuristic techniques to determine optimal placement of biomass power plants. Energy Conversion and Management 50 (8), 2020 – 2028.

Reklaitis, G. V., Khinast, J., Muzzio, F., 2010. Pharmaceutical engineering science - new

approaches to pharmaceutical development and manufacturing. Chemical Engineering Science 65, iv–vii.

Reynolds, G. K., Biggs, C. A., Salman, A. D., Hounslow, M. J., 2004. Non-uniformity of binder distribution in high-shear granulation. Powder Technology 140, 203–208.

Ronsse, F., Depelchin, J., Pieters, J. G., 2012. Particle surface moisture content estimation using population balance modelling in fluidised bed agglomeration. Journal of Food Engineering 109 (3), 347 – 357.

S., M. A., Ken, T. (Eds.), 1990. Crystallization as a Separations Process. American Chemical Society, Washington, DC.

Salman, A. D., Hounslow, M. J., Seville, J. P. K., 2007. Granulation. Elsevier.

Sastry, K. V., 1975. Similarity size distribution of agglomerates during their growth by coalescence in granulation or green pelletization. International Journal of Mineral Processing 2 (2), 187 – 203.

Seki, H., Furuya, N., Hoshino, S., 2012. Evaluation of controlled cooling for seeded batch crystallization incorporating dissolution. Chemical Engineering Science 77 (0), 10 – 17.

Seveno, D., Ledauphin, V., Martic, G., Voue, M., De Coninck, J., 2002. Spreading drop dynamics on porous surfaces. Langmuir 18 (20), 7496–7502.

Shi, Y., Eberhart, R., 1998. A modified particle swarm optimizer. In: Evolutionary Computation Proceedings, 1998. IEEE World Congress on Computational Intelligence., The 1998 IEEE International Conference on. pp. 69 –73.

Soos, M., Sefcik, J., Morbidelli, M., 2006. Investigation of aggregation, breakage and restructuring kinetics of colloidal dispersions in turbulent flows by population balance modeling and static light scattering. Chemical Engineering Science 61 (8), 2349 – 2363.

Stepanek, F., Rajniak, P., 2006. Droplet morphologies on particles with macroscopic surface roughness. Langmuir 22 (3), 917–923.

Stepanek, F., Rajniak, P., Mancinelli, C., Chern, R., Ramachandran, R., 2009. Distribution and accessibility of binder in wet granules. Powder Technology 189 (2), 376 – 384.

Tadayon, A., Rohani, S., Bennett, M. K., 2002. Estimation of nucleation and growth kinetics of ammonium sulfate from transients of a cooling batch seeded crystallizer. Industrial & Engineering Chemistry Research 41 (24), 6181–6193.

Thielmann, F., Naderi, M., Ansari, M. A., Stepanek, F., 2008. The effect of primary particle surface energy on agglomeration rate in fluidised bed wet granulation. Powder Technology 181 (2), 160 – 168.

Verkoeijen, D., Pouw, G. A., Meesters, G. M. H., Scarlett, B., 2002. Population balances for particulate processes–a volume approach. Chemical Engineering Science 57 (12), 2287 – 2303.

Walker, G. M., 2007. Chapter 4 drum granulation processes. In: A.D. Salman, M. H., Seville, J. (Eds.), Granulation. Vol. 11 of Handbook of Powder Technology. pp. 219 – 254.

Widenski, D., Abbas, A., Romagnoli, J., 2011. A model-based nucleation study of the combined effect of seed properties and cooling rate in cooling crystallization. Computers & Chemical Engineering 35 (12), 2696 – 2705.

Wnukowski, P., Setterwall, F., 1989. The coating of particles in a fluidized bed (residence time distribution in a system of two coupled perfect mixers). Chemical Engineering Science 44 (3), 493 – 505.